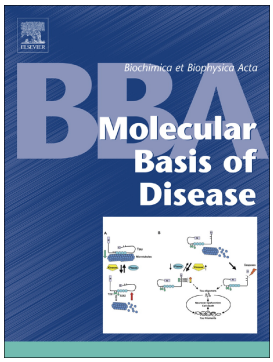

Proteomic identification of altered protein O-GlcNAcylation in in a triple transgenic mouse model of Alzheimer's disease

Antonella Tramutola, Nidhi Sharma, Eugenio Barone, Chiara Lanzillotta, Andrea Castellani, Federica Iavarone, Federica Vincenzoni, Massimo Castagnola, D. Allan Butterfield, Silvana Gaetani, Tommaso Cassano, Marzia Perluigi, Fabio Di Domenico

PII: S0925-4439(18)30260-6
DOI: doi:10.1016/j.bbadis.2018.07.017
Reference: BBADIS 65187

To appear in: *BBA - Molecular Basis of Disease*

Received date: 29 March 2018
Revised date: 22 June 2018
Accepted date: 16 July 2018

Please cite this article as: Antonella Tramutola, Nidhi Sharma, Eugenio Barone, Chiara Lanzillotta, Andrea Castellani, Federica Iavarone, Federica Vincenzoni, Massimo Castagnola, D. Allan Butterfield, Silvana Gaetani, Tommaso Cassano, Marzia Perluigi, Fabio Di Domenico , Proteomic identification of altered protein O-GlcNAcylation in in a triple transgenic mouse model of Alzheimer's disease. Bbadis (2018), doi:10.1016/j.bbadis.2018.07.017

Proteomic identification of altered protein O-GlcNAcylation in in a triple transgenic mouse model of Alzheimer's disease

Authors

Antonella Tramutola[1], Nidhi Sharma[1], Eugenio Barone[1,2], Chiara Lanzillotta[1], Andrea Castellani[1], Federica Iavarone[3], Federica Vincenzoni[3], Massimo Castagnola[3], D. Allan Butterfield[4], Silvana Gaetani[5], Tommaso Cassano[6], Marzia Perluigi[1] and Fabio Di Domenico[1#]

Affiliations

[1] *Department of Biochemical Sciences "A. Rossi Fanelli", Sapienza University of Rome, Rome, Italy*

[2] *Universidad Autònoma de Chile, Instituto de Ciencias Biomédicas, Facultad de alud, Providencia, Santiago, Chile*

[3] *Institute of Biochemistry and Clinical Biochemistry, Catholic University, Rome, Italy*

[4] *Department of Chemistry and Sanders-Brown Center on Aging, University of Kentucky, Lexington, KY, USA*

[5]*Department of Physiology and Pharmacology "V. Erspamer", Sapienza University of Rome, Rome, Italy.*

[6]*Department of Clinical and Experimental Medicine, University of Foggia, Foggia, Italy*

[#] Corresponding author:

Fabio Di Domenico, Ph.D

Department of Biochemical Sciences, Sapienza University of Rome

P.le Aldo Moro 5, Rome, Italy, 00185

fabio.didomenico@uniroma1.it

Keywords: Alzheimer disease, O-GlcNAcylation, phosphorylation, glucose metabolism, insulin signaling

Abstract

PET scan analysis demonstrated the early reduction of cerebral glucose metabolism in Alzheimer disease (AD) patients that can make neurons vulnerable to damage *via* the alteration of the hexosamine biosynthetic pathway (HBP). Defective HBP leads to flawed protein *O*-GlcNAcylation coupled, by a mutual inverse relationship, with increased protein phosphorylation on Ser/Thr residues. Altered *O*-GlcNAcylation of Tau and APP have been reported in AD and is closely related with pathology onset and progression. In addition, type 2 diabetes patients show an altered O-GlcNAcylation/phosphorylation that might represent a link between metabolic defects and AD progression. Our study aimed to decipher the specific protein targets of altered *O*-GlcNAcylation in brain of 12-month-old 3×Tg-AD mice compared with age-matched non-Tg mice. Hence, we analysed THE GLOBAL *O*-GLCNAC LEVELS, THE LEVELS AND ACTIVITY OF OGT and OGA, THE ENZYMES CONTROLLING ITS CYCLING AND PROTEIN SPECIFIC *O*-GlcNAc levels using a bi-dimensional electrophoresis (2DE) approach. Our data demonstrate the alteration of OGT and OGA activation coupled with the decrease of total *O*-GlcNAcylation levels. Data from proteomics analysis led to the identification of several proteins with reduced *O*-GlcNAcylation levels, which belong to key pathways involved in the progression of AD such as neuronal structure, protein degradation and glucose metabolism. In parallel, we analysed the *O*-GlcNAcylation/phosphorylation ratio of IRS1 and AKT, whose alterations may contribute to insulin resistance and reduced glucose uptake. Our findings may contribute to better understand the role of altered protein *O*-GlcNAcylation profile in AD, by possibly identifying novel mechanisms of disease progression related to glucose hypometabolism.

Introduction

The human brain constitutes only 2% of the body's mass but, under the basal condition, its metabolism accounts for up to 30% of the total body glucose uptake [1]. With the increase in age, brain glucose utilization declines to different degrees in different brain regions, and such decline is accelerated in Alzheimer disease (AD), for which ageing is the most important risk factor [1, 2]. A broad number of studies have proven the reduction of glucose uptake in the brain of AD patients [3, 4]. Alterations of brain glucose metabolism seems to occur also in subjects affected by mild cognitive impairment (MCI), prior to the appearance of clinical signs of dementia. Therefore, it is suggested this event is a cause, rather than a consequence of AD [5, 6]. Most of the glucose in the brain is oxidatively metabolized to produce ATP, to maintain neuronal activities and functions. However, approximately 2–5% of total glucose is also utilized in the hexosamine biosynthetic pathway (HBP) to produce glucosamine-6-phosphate and, ultimately, UDP-N-acetylglucosamine (UDP-GlcNAc) [1, 7]. UDP-GlcNAc is the donor substrate for *O*-linked-ß-N-acetylglucosamine transferase (OGT), which catalyses protein *O*-GlcNAcylation, a process transferring a single moiety of N-acetyl-D-glucosamine from UDP-GlcNAc to the hydroxyl side chains of serine and threonine residues of proteins. The reversible attachment of O-linked GlcNAc to proteins is catalyzed, beyond OGT, by *O*-GlcNAcase (OGA), which regulates its removal. The activation of OGT is sensitive to the amount of UDP-GlcNAc substrate and, therefore, to altered intracellular glucose metabolism [1, 5, 8-10].

Interestingly, *O*-linked N-acetylglucosaminylation (*O*-GlcNAcylation) and phosphorylation are mutually related. Indeed, several studies reported that *O*-GlcNAc can either occur in a reciprocal manner to serine (Ser) and threonine (Thr) phosphorylation or can interact with contiguous phosphorylated sites influencing their modification [10-13]. The crosstalk between *O*-GlcNAcylation and phosphorylation gives to *O*-GlcNAc the ability to modulate various phosphorylation-dependent signaling pathways known to be involve in cell development and homeostasis [14].

O-GlcNAcylation occurs in numerous cytoplasmic and nuclear proteins and recent studies have observed that the *O*-GlcNAcylation level of brain proteins, including tau, is dramatically decreased in AD, most likely as a result of decreased glucose metabolism and reduced HBP flux [1, 15-18]. Intriguingly, during AD progression brain *O*-GlcNAc levels appear to decrease while phosphorylation increases. Indeed, samples of frontal cortex from AD patients display significant reduction in global *O*-GlcNAc levels, but increased tau hyperphosphorylation as compared to controls [10, 19-21]. However, the reduction of total protein *O*-GlcNAcylation in AD is still a matter of controversy since other studies reported an inverse trend [2, 22, 23]. The abnormal phosphorylation/*O*-GlcNAcylation ratio of tau is critical to neurodegeneration, as increased

phosphorylation promotes tau aggregation into tangles, while higher levels of tau *O*-GlcNAcylation are protective against tangles formation [1, 5, 12, 16, 17, 24]. Immunofluorescent studies on human brain samples revealed an inverse relationship between tau *O*-GlcNAcylation and phosphorylation [1, 16]. As well, the presence of *O*-GlcNAc residues on the amyloid precursor protein (APP) has been reported suggesting that their alteration may be involved in the non-amyloidogenic processing of APP by γ-secretase [17, 25-28]. Increasing APP *O*-GlcNAcylation levels, by OGA inhibition, increases sAPPα levels and decreases Aβ levels, while alloxan, an OGA activator, reduces the *O*-GlcNAc levels of APP favoring Aβ production [27]. Further, nicastrin one of the components of the γ-secretase complex required for substrate recognition and binding [29], is modified by *O*-GlcNAc at Ser708, and this post translational modification (PTM) addition attenuates γ-secretase activity and prevents APP cleavage [28]. In addition, the increased *O*-GlcNAcylation of APP intensifies its trafficking rate from the trans-Golgi network to the plasma membrane and reduces its endocytosis rate [26]. Consequently, APP *O*-GlcNAcylation increases cell surface level of APP, resulting in decreased Aβ production. Thus, *O*-GlcNAcylation may also promote the plasma membrane localization of APP, which enhances its non-amyloidogenic processing. Studies conducted so far in AD considered mainly the aberrant *O*-GlcNAcylation of tau and APP supporting a role for this PTM in the formation of the plaques and tangles. However, the number of proteins targeted by *O*-GlcNAcylation is very high and its alteration could affect a number of different proteins involved in the neuropathological process during AD.

So far, treatments using inhibitors of OGA has been tested on different mouse models of AD or tauopathy showing in general that increasing the levels of *O*-GlcNAcylation is able to reduce disease hallmark and lower cognitive decline [27, 28, 30-32]. In particular, previous studies showed that chronic OGA inhibition resulted in reduced NFTs but not in the reduced phosphorylation of soluble tau, with the exception of Ser 400 which resulted hyper *O*-GlcNAcylated suggesting a role in hindering tau aggregation. As well, long-term OGA inhibition in AD mice led to reductions in the levels of AB in the brain and improved cognition. Recent data, suggest that OGA inhibitors may act through a mechanism involving the enhancement of autophagy, which aids the brain in the clearance of toxic protein species [33].

However, studies by others demonstrated that aberrant *O*-GlcNacylation could result detrimental for neurons independently from Aβ and tau and their rescue by OGA inhibitors may have beneficial effects in AD and also protects against both tau and Aβ toxicity [18].

The current study aimed to identify, by proteomics approach, the protein target of aberrant *O*-GlcNAcylation and conceivably understand their role in the development of AD neuropathology in the triple transgenic mouse model of AD (3×Tg-AD). Such model represents a valuable source to

comprehend the molecular mechanism that lead to AD development, since these mice develop age-related progressive neuropathology, including plaques and tangles, and brain insulin resistance [34]. In our previous glycoproteomics studies, we took advantage of lectin affinity to sugar moieties N- or *O*-linked to proteins in order to isolate specific glycoproteins and measure abundance difference between AD and CTR human IPL [35, 36]. Here, we employed a more selective antibody-related approach to selectively recognize *O*-GlcNAcylated proteins. Our analysis led to the identification of a number of proteins aberrantly *O*-GlcNAcylated whose altered functionality may actively contribute to the impairment of key pathways, such as energy production or neuronal architecture, associated with AD development and progression.

Materials and methods

Animals

Experiments were conducted on 6- and 12-month-old 3×Tg-AD (B6;129-Psen1^{tm1Mpm} Tg(APPSwe,tauP301L)1Lfa/Mmjax) male mice (6 mice per group) and on the corresponding non-Transgenic (Non-Tg) male littermates (6 mice per group). The 3xTg-AD mice harbor 3 mutant human genes (APP KM670/671NL (Swedish), MAPT P301L, PSEN1 M146V) and have been genetically engineered by La Ferla and colleagues [37]. The background strain of the mice is the C57BL6/129SvJ hybrid. The presence of mutations was confirmed using a PCR approach as previously reported [38, 39]. Colonies of homozygous 3xTg-AD and Non-Tg mice were established at the vivarium of Puglia and Basilicata Experimental Zooprophylactic Institute (Foggia, Italy). The housing conditions were controlled daily (temperature 22 °C, light from 07:00–19:00, humidity 50%–60%) and fresh food and water were freely available. All the experiments were performed in strict compliance with the Italian National Laws (DL 116/92), the European Communities Council Directives (86/609/EEC). All efforts were made to minimize the number of animals used in the study and their suffering. Animals were sacrificed at the selected age and the brain was extracted and divided according to its differential experimental utilization (1/2 brain, the left hemisphere was used for immunohistochemical analysis and therefore fixed in paraformaldehyde, while the other 1/2, the right hemisphere, was dissected and processed for biochemistry and molecular biology analysis). Fresh tissues were flash-frozen and stored at -80 °C until total protein extraction and further analyses were performed.

Sample preparation

Hippocampi from 3×Tg-AD and Non-Tg mice (n= 6 mice per group) were thawed in Media 1 lysis buffer (pH 7.4) containing: 320 mM Sucrose, 1% of 1 M Tris-HCl (pH = 8.8), 0.098 mM MgCl2, 0.076 mM EDTA, the proteinase and phosphatase inhibitors cocktail (Sigma-Aldrich, St Louis, MO, USA), PUGNAc (O-(2-Acetamido-2-deoxy-D-glucopyranosylidenamino) N-phenylcarbamate) [100 µM] and Benzyl-2-acetamol-2-deoxy- α -D-galactopyranoside [100 µM] (Sigma-Aldrich, St Louis, MO, USA), respectively OGA and OGT inhibitors. The brains were homogenized and sonicated and the resulting homogenates were centrifuged at 14,000×g for 10 min to remove debris. The supernatant was extracted to determine the total protein concentration by BCA method (Pierce Biotechnology, Rockford, IL, USA).

Two-dimensional (2D) electrophoresis and 2D blots

For the first-dimension electrophoresis, approximately 200 µl of sample (100 µg of proteins) from 3×Tg-AD and Non-Tg mice at 12 months of age were applied to 110-mm pH 3–10 IPG® ReadyStrip (Bio-Rad, Hercules, CA, USA). The strips were then actively rehydrated in the protean isoelectric focusing (IEF) cell (Bio-Rad, Hercules, CA, USA) at 50 V for 18 h. The isoelectric focusing was performed in increasing voltages as follows; 300 V for 1 h, then linear gradient to 8000 V for 5 h and finally 20000 V/h. Strips were then stored at −80 °C until the 2D electrophoresis was to be performed. For the second dimension, the IPG® Strips, were thawed and equilibrated for 10 min in 50 mM Tris–HCl (pH 6.8) containing 6 M urea, 1% (w/v) sodium dodecyl sulfate (SDS), 30% (v/v) glycerol, and 0.5% dithiothreitol, and then re-equilibrated for 15 min in the same buffer containing 4.5% iodacetamide instead of dithiothreitol. Linear gradient precast criterion Bis-Tris gels (12%) (Bio-Rad, Hercules, CA, USA) were used to perform second dimension electrophoresis. Precision Protein™ Standards (Bio-Rad, Hercules, CA, USA) were run along with the samples at 200 V for 50 min. After running the gels were incubated in fixing solution (10% acetic acid, 40% methanol) for 40 min and stained overnight at room temperature with 50 mL SYPRO Ruby gel stain (Bio-Rad, Hercules, CA, USA). The SYPRO ruby gel stain was then removed and gels stored in deionized water.

For 2D blots, gels were blotted on nitrocellulose membranes (Bio-Rad, Hercules, CA, USA) and glycoproteins were detected on the membranes. Briefly, membranes were blocked for 1 h with 3% albumin in T-TBS, incubated with a mix of two primary antibodies: *O*-GlcNAc RL-2 (#sc-59624, mouse, 1:1000; Santa Cruz, Biotechnology, Dallas, TX, USA) and CTD110.6 (#9875, mouse, 1: 500, Cell Signaling, Danvers, MA, USA) overnight at 4°C. After washing with T-TBS three times for 10 min, membranes were further incubated at room temperature for 1 h with the secondary antibody

alkaline phosphatase-conjugated anti-mouse IgG (1:5000; Sigma-Aldrich, St Louis, MO, USA). Membranes were then washed with T-TBS three times and developed using 5-bromo-4-chloro-3-indolyl phosphate/nitroblue tetrazolium solution (BCIP/NBT).

Image analysis

SYPRO ruby-stained gel and Blot images were obtained using a Chemidoc MP System (Bio-Rad, Hercules, CA, USA). All the images were saved in TIFF format. 2D gels and 2D blots images (12 gels and 12 blots) were analyzed by PD-Quest 2D Analysis (7.2.0 version; Bio-Rad, Hercules, CA, USA). PD-Quest spot-detection software allows the comparison of 2D gels as well as 2D blots, from 3×Tg-AD and Non-Tg groups. Briefly, a master gel was selected followed by normalization of all gels and blots (3×Tg-AD and Non-Tg) according to the total spot density. Gel-to-blot analysis was then initiated in two parts. First, manual matching of common spots was performed, that could be visualized among the differential 2D gels and 2D blots. After obtaining a significant number of spots the automated matching of all spots was then initiated. Automated matching is based on user-defined parameters for spot detection. These parameters are based on the faintest spot, the largest spot, and the largest spot cluster that occur in the master gel and are defined by the user. This process generates a large pool of data, approximately 400-800 spots. Only proteins showing computer-determined significant differential levels between the groups being analyzed were considered for identification.

To determine significant differential levels of proteins, analysis sets were created using the analysis set manger software incorporated into the PD-Quest software. The numbers of pixels that occur in a protein spot were computed by the software corresponding to an increase/decrease in protein level. The image analysis was conducted first on blot and then on Sypro Ruby-stained expression gels. The two analyses were compared by software to normalize glycosylation value to expression value for each spot matched.

In-gel trypsin digestion/peptide extraction

Protein spots identifies as significantly altered from the comparison of two groups (3×Tg-AD and Non-Tg mice) were excised from 2D-gels and transferred to individual Eppendorf microcentrifuge tubes for trypsin digestion as described previously. In brief, DTT and IA were used to break and cap disulfide bonds and the gel plug was incubated overnight at 37°C with shaking in modified trypsin solution. Tryptic peptide solutions were reconstituted in water and stored at −80° C until MS/MS analysis.

RP-HPLC-high resolution MS/MS characterization of tryptic peptides

High-resolution HPLC-ESI-MS/MS experiments were carried out by an Ultimate 3000 RSLC nano system coupled to an LTQ Orbitrap ELITE apparatus (Thermo Fisher Scientific, Waltham, MA, USA). Zorbax 300 SB-C18 (3.5 μm particle diameter; column dimension 1 mm × 150 mm) (Agilent Technologies, Santa Clara, CA, USA) was used as chromatographic column. The following eluents were used: (A) 0.1% (v/v) aqueous FA and (B) 0.1% (v/v) FA in ACN/water 80/20 v/v. The applied gradient was: 0-2 min 5% B, 2-40 min from 5 to 70% B (linear), 40-45 min from 70 to 99% B (linear), at a flow rate of 50 μL/min with a total run of 65 min. MS spectra were collected with 120,000 resolution and m/z range from 350 to 2000. In data-dependent acquisition mode the five most intense multiply-charged ions were selected and fragmented in ion trap by using CID 35% normalized collision energy. Tuning parameters were: capillary temperature 300 °C, source voltage 4.0 kV.

MS data analysis

MS/MS data were elaborated by Proteome Discoverer software (version 1.4.1.14, Thermo Fisher Scientific, Waltham, MA, USA), based on SEQUEST HT cluster as search engine against UniProtKB mouse database (released on 28 of February 2017, mus musculus 16839 entries). The search parameters were 10 ppm tolerance for precursor ions and 0.5 Da for product ions, 2 missed cleavage, carbamydomethylation of cysteine (+57.02 Da) as fixed modification, oxidation of methionine (+15.99 Da), *O*-GlcNac (+203,1950) as variable modification on Serine and Threonine. Protein characterization was set with the identification of a minimum of two peptides per protein and two unique peptides by applying the high confidence filter.

Immunofluorescence

Half mouse brain (left hemisphere) from each animal was removed and immersed in 4% paraformaldehyde 48 h. Fixed brains were cryoprotected in successive 72 h in 20% sucrose solution as described previously. Brains were frozen on a temperature-controlled freezing stage, coronal sectioned (20 μm) on a sliding microtome, and stored in a solution of PBS containing 0.02% NaN_3 at 4°C. Brain sections were mounted on glass slides with medium (30% ethanol in PBS). Once dry, sections were blocked and permeabilized in blocking buffer (10% normal goat serum and 0.2% Triton X-100 in TBS) for 2h. Slides were then incubated overnight at 4°C with following antibodies: *O*-GlcNAc RL-2 (#sc-59624; mouse 1:250, Santa Cruz, Biotechnology, Dallas, TX, USA) and CTD110.6 (#CST-9875; mouse 1:250, Cell Signaling, Danvers, MA, USA), total p-Thr (#sc-5267, mouse 1:250, Santa Cruz, Biotechnology, Dallas, TX, USA) and total p-Ser (#AB-9332, rabbit 1:500, Abcam, Cambridge, UK). Slides were washed with TBS and then incubated with Alexa Fluor 488nm

secondary antibody (#A10680, Fisher Molecular biology, Rome, Italy) at 1:1500 for 2 h at room temperature. Slides were then washed again and incubated with DAPI (1:10.000, Immunological Science, Rome, IT). One section from 3×Tg-AD and Non-Tg were stained omitting primary antibodies to establish nonspecific background signal. Cover slips were placed using a drop of Fluorimount (Sigma-Aldrich, St Louis, MO, USA).

OGA assay

OGA activity assay was performed using the synthetic substrate p-nitrophenyl N-acetyl-β-D-glucosaminide (pNP-GlcNAc) as described by Zachara et al. [40]. Briefly, samples were homogenized in isolation buffer without EDTA, EGTA and GlcNAc, and crude cytosolic fractions were prepared as described above. The samples were incubated with concanavalin A agarose for 30 minutes at 4°C to remove interfering hexosaminidases. Samples were then desalted using Zeba™ Desalt Spin Columns (Pierce Biotechnology, Rockford, IL, USA) and protein estimation was performed. Sample (25 µg) was mixed with activity assay buffer (final concentrations: 50 mM sodium cacodylate, pH 6.4, 50 mM N-acetylgalactosamine, 0.3% BSA, and 2 mM pNP-GlcNAc). Reactions were incubated at 37 °C for 2 h and stopped by the addition of 500 mM Na_2CO_3. Absorbance was read at 405 nm and OGA activity is reported as enzyme activity units where one unit catalyzes the release of 1 µmol pNP/min from pNP-GlcNAc.

Western blot

For western blot, 30 µg of proteins from hippocampus of 3×Tg-AD and Non-Tg at 6 and 12 months of age (n=6 mice per group) were separated by 12% SDS–PAGE, using new Criterion™ TGX (Tris-Glycine eXtended) Stain-Free™ precast gels. The long shelf life TGX formulation includes unique trihalo compounds that allow rapid fluorescent detection of proteins with ChemiDoc™ MP imaging systems. The resulting gel images correspond to the total load of proteins, which is further used to normalize all the blots. Once detected by ChemiDoc MP image system, the gels were transferred onto a nitrocellulose membrane (Bio-Rad, Hercules, CA, USA). Membrane were blocked with 3% bovine serum albumin in T-TBS and incubated overnight at 4°C with following primary antibodies: *O*-GlcNAc RL-2 (#sc-59624, 1:500, Santa Cruz, Biotechnology, Dallas, TX, USA), CTD110.6 (#9875, 1:1000, Cell Signaling, Danvers, MA, USA), OGA, (#SAB-4200267, 1:1000, Sigma–Aldrich, St Louis, MO, USA), OGT, Drp-2, Ulk1, p-Ser636 and total IRS1 (#sc-74546, #sc-30228, #sc-390904, #sc-33957, #sc-8038, 1:1000, Santa Cruz, Biotechnology, Dallas, TX, USA), Gapdh and Eno1 (#GTX-100118, #GTX-113179, GeneTex, Irvine, CA, USA), p-Ser473 Akt (#CST-4058, 1:1000, Cell Signaling, Danvers, MA, USA) and total Akt (#VMA-00253, 1:1000, Bio-Rad,

Hercules, CA, USA). Secondary antibodies horseradish peroxidase-conjugated anti-mouse or rabbit IgG (1:5000; Sigma–Aldrich, St Louis, MO, USA) were incubated for 1 h at room temperature. Membrane was developed with the Super Signal West Pico chemiluminescent substrate (Thermo Scientific, Waltham, MA, USA), acquired with ChemiDoc MP (Bio-Rad, Hercules, CA, USA) and analyzed using Image Lab software (Bio-Rad, Hercules, CA, USA).

Immunoprecipitation

The different samples-sets (100 µg of proteins) were incubated overnight with I.P. buffer (10mM Tris, pH 7.6; 140mM NaCl; 0.5% NP40 including protease inhibitors) and the following antibodies: OGT, Drp-2, Ulk1 (#sc-74546, #sc-30228, #sc-390904, 1:100, Santa Cruz, Biotechnology, Dallas, TX, USA), Gapdh and Eno1 (#GTX-100118, #GTX-113179, GeneTex, Irvine, CA, USA) followed by 2 h of incubation with Protein G beads (Sigma–Aldrich, St Louis, MO, USA) and then washed three times with RIA buffer (10mM Tris, pH 7.6; 140mM NaCl; 1% NP40). Proteins were separated by SDS-PAGE followed by immunoblotting on a nitrocellulose membrane (Bio-Rad, Hercules CA, USA). Membrane were incubated with the antibodies anti-*O*-GlcNAc RL-2 (#sc-59624, mouse, 1:500, Santa Cruz, Biotechnology, Dallas, TX, USA) and CTD110.6 (#9875, mouse, 1:500, Cell Signaling, Danvers, MA, USA), total p-Thr (#sc-5267, mouse 1:250, Santa Cruz, Biotechnology, Dallas, TX, USA) and total p-Ser (#AB-9332, rabbit 1:500, Abcam, Cambridge, UK) and then detected by the peroxidase-conjugated secondary antibody (1:5000; Sigma–Aldrich, St Louis, MO, USA) with Super Signal West Pico chemiluminescent substrate (Thermo Scientific, Waltham, MA, USA). Membranes were then acquired with ChemiDoc MP image system (Bio-Rad, Hercules, CA, USA) and analyzed using Image Lab software (Bio-Rad, Hercules, CA, USA). The IP results were normalized on the total amount of the proteins of interest.

Statistical analysis

Data obtained by PD-QUEST software were compared using Student's t-test. Significance was accepted if the p value < 0.05. All the data are expressed as mean ± SEM of 6 independent samples per group. All statistical analyses were performed using GraphPad Prism 5.0 software.

Results

3×Tg-AD mice represent a valuable model for the study of *O*-GlcNAcylation since previous studies demonstrated that they develop an age-related reduction of brain glucose uptake, together with age-related insulin resistance and decreased expression of the type-3 neuronal glucose

transporter (GLUT-3) [41, 42]. Further, those mice do not show neuronal loss suggesting that variation of protein *O*-GlcNAcylation should be driven by altered glucose metabolism [37]. Earlier findings by Gatta and collaborators reported that 12-month-old 3×Tg-AD mice show reduced tau *O*-GlcNAcylation associated with increased tau hyperphosphorylation in the hippocampus [19]. Interestingly, the reduction of tau *O*-GlcNAcylation is region-specific and did not occur in the cortex, as also observed by us (Sup. Fig. 1), or cerebellum. Further, the authors demonstrated that the selective reduction in tau *O*-GlcNAcylation, found in the hippocampus of 12-month-old 3×Tg-AD mice, was in line with the pattern of tau pathology observed in these mice.

Before performing our proteomic analysis, we decided to explore the decrease of total protein *O*-GlcNAcylation and increased tau phosphorylation in 3×Tg-AD mice compared to Non-Tg mice at two different ages, 6 months and 12 months (Sup. Fig. 2). The age of 6 months represents an early phase of the neurodegenerative process in the 3×Tg-AD mice, while 12-month-old animals are crucial to demonstrate a robust alteration of *O*-GlcNAcylation and phosphorylation [34]. Noteworthy, hippocampus homogenates were analysed in the presence of OGT and OGA inhibitors. We found that the use of inhibitors is a key step during sample preparation in order to obtain reliable and reproducible data [40]. Conflicting data, about *O*-GlcNAcylation levels in AD human and mouse brain, may depend on the accuracy of the sample preparation and the lack of specific inhibitors in the sample homogenate. In addition, to obtain a broad range of data on protein aberrantly glycosylated we decided to use a mix of two antibodies (CTD110.6 and RL2 recognizing both low and high molecular weight *O*-GlcNAcylated proteins only, as demonstrated by us (Fig.1 A; Sup. Fig. 3) and others [2, 19]. As expected, western blotting data revealed a consistent decrease in total protein *O*-GlcNAc levels in 12-month-old 3×Tg-AD mice (about 0.3-fold vs. Non-Tg mice), which correlates with tau hyperphosphorylation (Fig. 1 A-E), while no difference between genotype was observed in 6-month-old mice (Sup. Fig. 1). Subsequently, we analysed total levels of *O*-GlcNAcylated proteins in parallel with total protein Ser/Thr phosphorylation by immunofluorescence in 12-month-old 3×Tg-AD mice brain (Fig. 1D). Our data show decreased *O*-GlcNAc levels in the CA3 region of the hippocampus of 3×Tg-AD mice (Fig. 1D 1-4), accompanied by an increase of serine and threonine phosphorylation (Fig. 1D 5-8). These data support an evident degree of inverse relationship between *O*-GlcNAcylation and phosphorylation in the proteome of hippocampal neurons. Indeed, the correlation analysis between total protein *O*-GlcNAcylation and total protein Ser/Thr phosphorylation in 3×Tg-AD mice demonstrate a significant negative correlation (R squared=0.852; p=0.025) while no correlation is shown for Non-Tg animals (Fig. 1E).

In order to explore the causes that lead to reduced protein *O*-GlcNAcylation in AD mice we further investigated the protein levels and activation status of the enzymes involved in the process of

removal and addition of *O*-GlcNAc residues to proteins: OGA and OGT (Fig. 2). The analysis of OGA demonstrated that protein levels did not change in 12-month-old 3×Tg-AD mice compared to age-matched Non-Tg mice, however in the same animals we showed an increase of OGA enzyme activity in the transgenic mice (Fig. 2 A, B). This result is in line with the observed reduction of protein *O*-GlcNAcylation. The analysis of OGT levels demonstrates, as well, no changes between AD mice compared to Non-Tg mice. As far as OGT, previous studies demonstrated no alterations in enzyme activity in 3×Tg-AD mice compared to Non-Tg [19], We analysed its phosphorylation/*O*-GlcNAcylation ratio, which may control, beyond enzyme activity, also its substrates recognition and/or its translocation from nucleus to plasma membrane [43-46]. Our results show an increase for OGT total Ser/Thr phosphorylation of about 2-fold but not significant alterations of specific *O*-GlcNAcylation of OGT in 12-month-old 3×Tg-AD mice (Fig. 2 C, D). Overall, the analysis of OGA and OGT enzymes suggests the involvement of these two enzymes in the reduction of total protein *O*-GlcNAcylation in AD pathology.

After having confirmed the reduction of *O*-GlcNac in AD, driven by the aberrant activity of OGT and OGA enzyme activation, we performed proteomics analysis of *O*-GlcNAcylated targets in order to identify specific proteins with altered *O*-GlcNAc levels in AD mice compared to Non-Tg mice. Our analysis allowed the identification of 14 proteins differentially *O*-GlcNAcylated (normalized on protein levels) (Fig. 3A and Table 1). Proteins identified by mass spectrometry were: Elongin-C (ELOC) (DNA and RNA regulation) with 4.1-fold decrease; Glyceraldehyde 3-phosphate dehydrogenase (Gapdh) (Glucose metabolism) with 7.1-fold decrease; GTP-binding nuclear protein Ran (Ran) (Energy metabolism) with 5.2-fold decrease; Ser/Thr-protein kinase Ulk1 (autophagy) with 2.1-fold decrease; putative ATP-dependent RNA helicase TDRD9 (TDRD9) (DNA and RNA regulation) with 4.1-fold decrease; Myosin phosphatase Rho-interacting protein (Mprip) (Cytoskeletal network) with 5.0-fold decrease; Tubulin α-1C chain (Tuba1c) with 10.0-fold decrease; α-enolase (Eno1) (Glucose metabolism) with 9.0-fold decrease; Dihydropyrimidinase-related protein 2 (Drp-2) (Neurotransmission) with 2.0-fold decrease; malate dehydrogenase (Mdh) (Glucose metabolism) with 4.3-fold decrease; Contactin-associated protein like 2 (Cntnap2) (Neurotransmission) with 14.2-fold decrease; Coiled-coil domain-containing protein 63 (Ccdc63) (Cytoskeletal network) with 2.1-fold decrease; 14-3-3 protein epsilon (14-3-3 E) (cell signaling) with 6.25-fold decrease and Neurofilament light polypeptide (NF-L) (Cytoskeletal network) with 3.3-fold decrease. It is interesting to notice that all the proteins show a decrease of *O*-GlcNAc modification in agreement with the total reduction previously observed (Table 1).

Further, to confirm that our method recognized *O*-GlcNAcylated proteins and that proteomics data are reliable, we performed validation analysis on four of the proteins found to be aberrantly *O*-

GlcNAcylated, Drp-2, Ulk1, Eno1 and Gapdh (Fig 4). Samples were immunoprecipitated by specific antibodies and analysed for *O*-GlcNAc levels by western blot using both RL2 and CTD110.6 antibodies. The western blot confirmed proteomics analysis showing a reduction of *O*-GlcNAcylation for Drp-2, Ulk1, Eno1 and Gapdh (0.7 –fold, 0.75-fold, 0.4-fold and 0.3-fold respectively) (Fig. 4 A-D). Since reduced *O*-GlcNAc levels may affect protein phosphorylation on Ser/Thr residue, we analysed in parallel the total Ser/Thr phosphorylation levels of identified protein in 3×Tg-AD mice. Our data show no significant alteration for Drp-2, Ulk1 and Eno1 while a trend of increase (about 1.5-fold, not significant) might suggest a mutual relationship between O-GlcNacylation and phosphorylation (Fig. 4 A-D).

Various studies have shown that *O*-GlcNAcylation of insulin signaling components is altered during AD and could be involved in energy failure, neuronal dysfunction and plaques and tangles formation [3, 6, 47]. IRS1 is a key player for insulin signaling and is a one of the downstream messengers of the insulin receptor. We found that *O*-GlcNAcylated IRS1 show a trend of decrease in the hippocampus of 12-month-old 3×Tg-AD compared to Non-Tg mice, which however is not significant (Fig 5). In parallel the analysis of IRS1 phosphorylation on an inhibitory residue, Ser636, demonstrate an increase of about 1.6-fold in 3×Tg-AD compared to Non-Tg mice. Our data demonstrate that increased phosphorylation of a single Ser residue of IRS1 is not coupled by the reduction of total Ser/Thr *O*-GlcNAcylation. (Fig. 5 A-C). Akt is a well-known Ser/Thr kinase enzyme involved in PI3K/Akt signaling pathway in the response of insulin signaling [47]. Our western blot analysis shows surprisingly significantly increased *O*-GlcNAcylated Akt in the hippocampus of 12-month-old 3×Tg-AD mice compared to Non-Tg mice (about 2-fold, Fig 5), which negatively correlates with the decrease of the phosphorylation levels at Ser473 (about 0.5-fold) (Fig. 5 D-F). Overall, these findings suggest that high level of *O*-GlcNAcylation may modulate protein phosphorylation, as Akt activation, therefore the occurrence of *O*-GlcNAcylation event would likely to contribute to the alteration of downstream regulatory pathway leading towards AD pathology.

Discussion

Protein *O*-GlcNAcylation is a ubiquitous PTM in living systems that appears to regulate more that 3000 proteins involved in transcription, protein translation and degradation, cell signaling among others [7-9, 14, 48, 49]. Remarkably, despite its abundance, *O*-GlcNAcylation is regulated primarily by the action of only two enzymes OGT and OGA whose expression is up to 10-times higher in brain compared to peripheral tissue, therefore suggesting that *O*-GlcNAcylation plays an important role in neuronal signaling [18]. In a previous study performed on 12-months-old 3×Tg-AD mice, it was shown a hippocampus-specific reduction of protein *O*-GlcNAcylation compared with Non-Tg

animals [19]. Our data confirm that total protein *O*-GlcNAcylation is reduced in 12-month-old 3×Tg-AD mice compared to Non-Tg with the concomitant increase of Ser/Thr phosphorylation levels. The analysis of OGT and OGA expression levels and regulation suggests the involvement of an aberrant activation of these enzymes during AD. Indeed, despite unchanged protein levels we observed an increase of OGA enzyme activity, which could translate as an increased removal of GlcNAc residues from proteins, as well as aberrant OGT phosphorylation/*O*-GlcNAcylation ratio which may regulate OGT activity, as well, as its substrate recognition or translocation to the plasma membrane [44, 45]. Previous studies suggested a direct association between reduced glucose uptake, which has been observed in 3×Tg-AD mice [19, 41, 42], altered insulin signalling and aberrant OGT PTMs [46, 50]. Further, it was demonstrated that increased OGT phosphorylation may be related to GSK3ß kinase activity [43, 50], which is increased in AD pathology comprising 3×Tg-AD mice [39], or to AMPK activation [44]. Despite other did not observed altered OGT activity in 3×Tg-AD mice [19], we suggest that its aberrant phosphorylation might result in altered nucleoplasmic localization or substrate binding.

The involvement of an aberrant HBP and protein *O*-GlcNAcylation in reduced glucose utilization and impaired insulin signaling has been extensively demonstrated by several authors in different tissues including the brain [1, 3, 16, 43]. Indeed, if on one hand the reduction of glucose entry in the cell, leads to reduced UDP-GlcNAc substrate availability and altered OGT activity, on the other side the reduction of protein *O*-GlcNAcylation can deregulate several proteins involved in glucose transport and catabolism [1, 3, 6, 14-16, 51]. Interestingly, we identified by a proteomics approach the altered *O*-GlcNAcylation of three components of the glucose metabolic pathway, two enzymes involved into glycolysis, Gapdh and enolase, and one enzyme involved in Krebs cycle, Mdh. Gapdh has catalytic role in the formation of 1,3 di-phosphoglycerate from glyceraldehyde 3-phosphate. In addition, Gapdh also can exert a phosphotransferase/kinase activity [52]. This enzyme presents in its amino acidic sequence several Ser/Thr residues that can be either *O*-GlcNAcylated or phosphorylated [53]. Previous studies showed that Gapdh activity could be regulated by various cellular kinases including, protein kinase C, epidermal growth factor kinase, and Ca2+/calmodulin-dependent protein kinase II, which may work in opposition to OGT in controlling the activation of the enzyme [54, 55]. Enolase catalyses the formation of phosphoenolpyruvate from 2-phosphoglycerate, while malate dehydrogenase catalyses the oxidation of malate to oxaloacetate. Likewise, enolase and Mdh contain in their amino acidic sequences several Ser/Thr residues that can be modified by either *O*-GlcNAcylation or phosphorylation [56, 57]; however, it has not been clarified yet how the modulation of these sites can influence Eno1 and Mdh function. Overall, our findings suggest in an AD model a potential role of *O*-GlcNAc modification in mediating Gapdh,

Eno1 and Mdh activity during glycolysis and the Krebs cycle. It is tempting to speculate that the impairment of these glucose-related enzymes may contribute to the reduction of glucose metabolism and ATP production in the brain, which in turn leads to altered protein *O*-GlcNAcylation, therefore generating a vicious cycle of events that lead to neurodegeneration. However, further knowledge on the residues modified by *O*-GlcNAc is required in order to understand the exact mechanisms linking protein *O*-GlcNAcylation to altered protein activity.

Our data are supported by a previous study using iTRAQ proteomics approach on synaptosomes and post-synaptic densities isolated from human AD and control frontal cortex [58]. The authors demonstrated altered *O*-GlcNAcylation of Gapdh and Mdh enzymes, observing a decreased in AD samples compared to CTRs [58]. Considering the mutual relationship between *O*-GlcNAcylation and phosphorylation, an indirect confirmation of our results on Gapdh, Eno1 and Mdh can be obtained by published phosphoproteomics analysis. Indeed, previous studies from our laboratory showed, in the hippocampus of AD patients compared to healthy subjects, increased phosphorylation levels for Eno1 and Gapdh suggesting a deregulation of such enzymes during neurodegeneration [59]. Further, phosphoproteomics analysis in AD human cortex and substantia nigra confirmed the hyperphosphorylation of Gapdh and proposed the hyperphosphorylation of Mdh enzyme [60, 61]. In addition, it is also critical to note that components of the glycolysis pathways and of the Krebs cycle are targeted by reactive oxygen species during AD leading to protein oxidation and reduced energy metabolism [62]. Within this context our data about the altered *O*-GlcNAcylation of enzymes involved in energy production, could add a further piece to the puzzle regarding the molecular mechanisms that lead to energy failure in AD. In agreement with our hypothesis, previous studies found the decreased *O*-GlcNAcylation of ATP5A in AD human tissue and in an AD mouse model [63], supporting the involvement of aberrant *O*-GlcNAcylation in the reduction of ATP production.

Notwithstanding our proteomics analysis did not result in the identification of altered *O*-GlcNAcylation of any component of the insulin signaling pathway, due to the direct relationship between reduced glucose uptake and insulin signaling and to the pivotal role of insulin cascade in mediating synaptic plasticity in the brain [3, 16, 64, 65], we investigated the aberrant *O*-GlcNAcylation of IRS1 and Akt [66]. The identification of glucose transporters regulated by insulin on brain cells confirmed that metabolic control is essential for brain function [67]. In addition, previous studies suggested a role for OGT, when active, as a regulator of insulin signaling [68]. High levels of glucose in the cell lead to increased levels of OGT substrate UDP-GlcNAc, which in turn increase the activation of the OGT enzyme activity [69]. OGT, which possesses a PIP_3 recognition sequence, is partially re-localized at the plasma membrane following PI3 kinase activation by insulin.

At the plasma membrane, OGT induces *O*-GlcNAcylation of proximal elements of insulin signaling, such as IRS, PI3K, and Akt resulting in signal regulation [68]. During AD, neurons face an opposite situation, in which reduced glucose metabolism leads supposedly to reduced OGT activity and reduced *O*-GlcNAcylation of insulin signaling components. The first component of the insulin signaling that we analysed was the insulin receptor substrate, which is involved in the activation of the PI3K pathway. IRS1 activity is regulated by its phosphorylation at multiple sites in either activating or inhibiting way. Previous studies from our laboratory demonstrated that triple transgenic AD mouse at 12 months of age showed increased phosphorylation of IRS1 at the inhibitory residue Ser 307, while no alteration in the activating residue tyrosine 632 was shown, supporting the reduced activity of IRS1 at this time point during AD pathology [34]. We hypothesize that increased IRS1phosphorylation at the inhibitory Ser307 is accompanied by the reduction of *O*-GlcNAc levels due reduced glucose metabolism. Our data demonstrate indeed a parallel reduction of *O*-GlcNAcylated IRS1 Ser/Thr residues, which negatively correlates with the increase of IRS1 phosphorylation at Ser 636, a further inhibitory site. Predictive studies on alternate phosphorylation/*O*-GlcNAcylation levels of IRS1 support the mutual exclusive relationship in the inhibitory Ser residue 307 and 636, suggesting that the reduced *O*-GlcNAcylation of IRS1 may contribute to its increased phosphorylation on its inhibitory site and to its inactivation [51, 70].

A second key regulator of the insulin signaling is Akt, which is activated by PDK1 under the control of PI3K. Akt is a key signaling player in the neuron being involved in the regulation of GSK3β kinase activity, apoptosis, CREB and mTOR signaling, among others. The activity of Akt is regulated by phosphorylation at Ser 473; however, several studies showed that when *O*-GlcNAcylation occurs Akt activation is reduced [47, 66, 71]. Our data show that in 3×Tg-AD mice the increase of Akt *O*-GlcNAc glycosylation is concomitant with reduced phosphorylation of Akt at Ser 473, putatively resulting in reduced activity. Intriguingly, reduced activation of Akt is in line with the reported increase of GSK3β activation in 3×TgAD mice and in AD patients. A further intriguing characteristic of *O*-GlcNAcylation-mediated Akt regulation is the increase of N-acetylglucosamine levels of Akt despite reduced glucose metabolism, which has not been observed for any other protein during our study. Such behaviour may be explained with a probable regulatory role of OGT in Akt *O*-GlcNAcylation. Indeed, OGT, but not OGA, is recruited with Akt to the cytoplasmic membrane where it has direct access to Akt and can catalyses its *O*-GlcNAcylation [71, 72].

A further interesting outcome of our proteomic analysis is the reduced O-GlcNAcylation of proteins implicated in the formation and maintenance of neuronal structure and architecture. As previously stated, the imbalanced regulation of tau *O*-GlcNAcylation/phosphorylation ratio is a key contributor to NTF formation during AD [5, 10, 21, 24]. Our results report the altered *O*-

GlcNAcylation of α-tubulin, which is directly involved, by interacting with β tubulin, in the organization of microtubules heterodimers. Microtubule structure is known to be impaired in AD and in addition to tau hyperphosphorylation, altered PTMs of α- and β-tubulin have been observed. Previous analysis demonstrated that together with reduced α-tubulin levels, also acetylated tubulin, polyglutamylated tubulin, tyrosinated tubulin, and detyrosinated tubulin were significantly decreased in AD brain [73]. As far as phosphorylation/*O*-GlcNAcylation ratio of Ser/Thr residues heterodimers structure, only phosphorylation on Ser172 of β-tubulin has been recognized as crucial in the formation of microtubules, however several others Ser residues might be the target of *O*-GlcNAcylation or phosphorylation [74, 75].

Another component of the neuron cytoskeleton, identified with reduced *O*-GlcNAcylation by proteomics analysis in 3×Tg-AD mice is the neurofilament light chain (NF-L) that is part of the intermediate filaments family. Neurofilaments are believed to function primarily to provide structural support for the axon and to regulate axonal diameter [11]. Neurofilaments are composed by subunits that belong, in mature neurons, to three class of proteins, the light chain, the medium chain and the heavy chain. Those three class of subunits interacting together form the neurofilament triplets, which in mature neurons co-polymerized with α internexin, a fourth class of protein. Neurofilament proteins are extensively modified by both *O*-GlcNAcylation and phosphorylation [96,97]. Altered phosphorylation of neurofilaments may precede their accumulation in axons [99], while increased *O*-GlcNAc levels may play, as discussed for tau, a protective role for NFT formation [11]. Our proteomics data are in line with previous reports supporting the reduced *O*-GlcNAcylation of NF-L in transgenic mice of AD.

Drp-2 is expressed in the nervous system during development and plays an important role in neurite extension and in axon guidance through the interactions with microtubules. In particular, Drp-2 is able to bind and copolymerize with tubulin heterodimers. Proteomics studies on rat synaptosomes demonstrated that during physiological condition Drp-2 is highly *O*-GlcNAcylated [76]. In contrast, several phosphoproteomics studies highlighted that in AD brain, Drp-2 undergoes hyperphosphorylation and it is associated with NFT [59, 60, 77]. Drp-2 hyperphosphorylation inactivates the protein by lowering the binding affinity to tubulin. In particular, Drp-2 phosphorylation at specific Ser/Thr residues has been linked to the degenerating neurites in AD [78]. Indeed, studies suggest that GSK3β and cyclin-dependent protein kinase 5 (Cdk5), highly expressed in AD, are some of the protein kinases responsible for inactivating Drp-2 in AD [79]. Unexpectedly, despite the reduction of *O*-GlcNAcylation, we did not observe an opposite increase of phosphorylation in our samples. This event may be explained with the high number of Ser/Thr residues that could undergoes to *O*-GlcNAcylation/phosphorylation mutual exchange or not. If the

second case occurs, data will result in unaltered phosphorylation levels. However, a systematic analysis of all Drp-2 Ser/Thr residues would be needed.

A foster intriguing result of our proteomics analysis regards the altered *O*-GlcNAcylation of Ulk1 protein, a key component of the autophagy lysosome pathway (ALS). The induction of ALS, which is involved in degradation of protein aggregates and organelles, is largely known to be reduced in AD human samples as well as mouse models of the disease comprising the 3×Tg-AD [80-82]. mTOR is the master regulator of autophagy and during physiological conditions mTOR responds to a nutrient-rich environment by hyperphosphorylating Ulk1, leading to the inactivation of its complex, thus impeding autophagosome formation and autophagy flux [83]. In the case of starvation, conversely, AMPK inhibits mTOR leads to the activation of the Ulk1 complex and induces the autophagy lysosome pathway [84]. During AD, a chronic hyperphosphorylation of mTOR and inactivation of Ulk1 has been observed [85]. Ulk1 phosphorylation by mTOR is in line with its reduced *O*-GlcNAc levels observed in this study, suggesting that *O*-GlcNAcylation of Ulk1 could represent a protective mechanism for autophagy induction. In addition, previous studies demonstrated that in addition to Ulk1, other components of the autophagy pathway, such as LC3-II expression, are sensitive to modulation of *O*-GlcNAcylation levels [33, 84]. Therefore, *O*-GlcNAcylation appears to be critical in regulating autophagy and may be involved in the increased proteotoxicity observed during neurodegenerative diseases.

Finally, we analysed our data by building a protein interaction map using STRING software (version 10.5) in order to understand the potential relationships among the proteins found altered in *O*-GlcNAcylation and the potential effects of their impaired function [86, 87]. As expected, a strong interaction is evident between the three components of the glycolysis pathway and Krebs cycle suggesting their cross talk in mediating the failure of glucose metabolism in AD. Intriguingly, the interaction between Gapdh and α-tubulin has been previously postulated [52], suggesting that Gapdh mediates tubulin phosphorylation and catalyses microtubule formation and polymerization (details are reported in Fig.6).

In conclusion, the proteins showing aberrant *O*-GlcNAcylation levels in 3×Tg-AD mice are involved in energy metabolism, insulin signaling, neuronal structure and autophagy among others. These pathways have pivotal roles in neuronal processes that are known to be impaired in AD; however, our data also allowed to gain further insights into the mechanisms that lead to their alterations. Within this context, our results may favour, conceivably, the identification of further pharmacological targets that can lead to reduced brain damage and cognitive decline.

Acknowledgements

This work was supported by Ministry of Instruction, University and Research (MIUR) under the SIR program n° RBSI144MT and Fondi di Ateneo from Sapienza University of Rome to FDD;

References

[1] F. Liu, J. Shi, H. Tanimukai, J. Gu, J. Gu, I. Grundke-Iqbal, K. Iqbal, C.X. Gong, Reduced O-GlcNAcylation links lower brain glucose metabolism and tau pathology in Alzheimer's disease, Brain, 132 (2009) 1820-1832.
[2] S. Forster, A.S. Welleford, J.C. Triplett, R. Sultana, B. Schmitz, D.A. Butterfield, Increased O-GlcNAc levels correlate with decreased O-GlcNAcase levels in Alzheimer disease brain, Biochim Biophys Acta, 1842 (2014) 1333-1339.
[3] S. Hoyer, Glucose metabolism and insulin receptor signal transduction in Alzheimer disease, Eur J Pharmacol, 490 (2004) 115-125.
[4] G.S. Smith, M.J. de Leon, A.E. George, A. Kluger, N.D. Volkow, T. McRae, J. Golomb, S.H. Ferris, B. Reisberg, J. Ciaravino, et al., Topography of cross-sectional and longitudinal glucose metabolic deficits in Alzheimer's disease. Pathophysiologic implications, Arch Neurol, 49 (1992) 1142-1150.
[5] C.X. Gong, F. Liu, K. Iqbal, O-GlcNAcylation: A regulator of tau pathology and neurodegeneration, Alzheimers Dement, 12 (2016) 1078-1089.
[6] Y. Yu, X. Li, J. Blanchard, Y. Li, K. Iqbal, F. Liu, C.X. Gong, Insulin sensitizers improve learning and attenuate tau hyperphosphorylation and neuroinflammation in 3xTg-AD mice, J Neural Transm (Vienna), 122 (2015) 593-606.
[7] R.J. Copeland, G. Han, G.W. Hart, O-GlcNAcomics--Revealing roles of O-GlcNAcylation in disease mechanisms and development of potential diagnostics, Proteomics Clin Appl, 7 (2013) 597-606.
[8] B.D. Lazarus, D.C. Love, J.A. Hanover, O-GlcNAc cycling: implications for neurodegenerative disorders, Int J Biochem Cell Biol, 41 (2009) 2134-2146.
[9] K. Vaidyanathan, S. Durning, L. Wells, Functional O-GlcNAc modifications: implications in molecular regulation and pathophysiology, Crit Rev Biochem Mol Biol, 49 (2014) 140-163.
[10] Y. Yu, L. Zhang, X. Li, X. Run, Z. Liang, Y. Li, Y. Liu, M.H. Lee, I. Grundke-Iqbal, K. Iqbal, D.J. Vocadlo, F. Liu, C.X. Gong, Differential effects of an O-GlcNAcase inhibitor on tau phosphorylation, PLoS One, 7 (2012) e35277.
[11] Y. Deng, B. Li, F. Liu, K. Iqbal, I. Grundke-Iqbal, R. Brandt, C.X. Gong, Regulation between O-GlcNAcylation and phosphorylation of neurofilament-M and their dysregulation in Alzheimer disease, FASEB J, 22 (2008) 138-145.
[12] X. Li, F. Lu, J.Z. Wang, C.X. Gong, Concurrent alterations of O-GlcNAcylation and phosphorylation of tau in mouse brains during fasting, Eur J Neurosci, 23 (2006) 2078-2086.
[13] J.C. Trinidad, D.T. Barkan, B.F. Gulledge, A. Thalhammer, A. Sali, R. Schoepfer, A.L. Burlingame, Global identification and characterization of both O-GlcNAcylation and phosphorylation at the murine synapse, Mol Cell Proteomics, 11 (2012) 215-229.
[14] Q. Zeidan, G.W. Hart, The intersections between O-GlcNAcylation and phosphorylation: implications for multiple signaling pathways, J Cell Sci, 123 (2010) 13-22.
[15] W.B. Dias, G.W. Hart, O-GlcNAc modification in diabetes and Alzheimer's disease, Mol Biosyst, 3 (2007) 766-772.
[16] Y. Liu, F. Liu, I. Grundke-Iqbal, K. Iqbal, C.X. Gong, Brain glucose transporters, O-GlcNAcylation and phosphorylation of tau in diabetes and Alzheimer's disease, J Neurochem, 111 (2009) 242-249.

[17] B.W. Zheng, L. Yang, X.L. Dai, Z.F. Jiang, H.C. Huang, Roles of O-GlcNAcylation on amyloid-beta precursor protein processing, tau phosphorylation, and hippocampal synapses dysfunction in Alzheimer's disease, Neurol Res, 38 (2016) 177-186.
[18] Y. Zhu, X. Shan, S.A. Yuzwa, D.J. Vocadlo, The emerging link between O-GlcNAc and Alzheimer disease, J Biol Chem, 289 (2014) 34472-34481.
[19] E. Gatta, T. Lefebvre, S. Gaetani, M. dos Santos, J. Marrocco, A.M. Mir, T. Cassano, S. Maccari, F. Nicoletti, J. Mairesse, Evidence for an imbalance between tau O-GlcNAcylation and phosphorylation in the hippocampus of a mouse model of Alzheimer's disease, Pharmacol Res, 105 (2016) 186-197.
[20] S.A. Yuzwa, A.H. Cheung, M. Okon, L.P. McIntosh, D.J. Vocadlo, O-GlcNAc modification of tau directly inhibits its aggregation without perturbing the conformational properties of tau monomers, J Mol Biol, 426 (2014) 1736-1752.
[21] F. Liu, K. Iqbal, I. Grundke-Iqbal, G.W. Hart, C.X. Gong, O-GlcNAcylation regulates phosphorylation of tau: a mechanism involved in Alzheimer's disease, Proc Natl Acad Sci U S A, 101 (2004) 10804-10809.
[22] M. Frenkel-Pinter, M.D. Shmueli, C. Raz, M. Yanku, S. Zilberzwige, E. Gazit, D. Segal, Interplay between protein glycosylation pathways in Alzheimer's disease, Sci Adv, 3 (2017).
[23] L.S. Griffith, B. Schmitz, O-linked N-acetylglucosamine is upregulated in Alzheimer brains, Biochem Biophys Res Commun, 213 (1995) 424-431.
[24] K. Iqbal, F. Liu, C.X. Gong, Tau and neurodegenerative disease: the story so far, Nat Rev Neurol, 12 (2016) 15-27.
[25] Y.S. Chun, O.H. Kwon, S. Chung, O-GlcNAcylation of amyloid-beta precursor protein at threonine 576 residue regulates trafficking and processing, Biochem Biophys Res Commun, 490 (2017) 486-491.
[26] Y.S. Chun, Y. Park, H.G. Oh, T.W. Kim, H.O. Yang, M.K. Park, S. Chung, O-GlcNAcylation promotes non-amyloidogenic processing of amyloid-beta protein precursor via inhibition of endocytosis from the plasma membrane, J Alzheimers Dis, 44 (2015) 261-275.
[27] K.T. Jacobsen, K. Iverfeldt, O-GlcNAcylation increases non-amyloidogenic processing of the amyloid-beta precursor protein (APP), Biochem Biophys Res Commun, 404 (2011) 882-886.
[28] C. Kim, D.W. Nam, S.Y. Park, H. Song, H.S. Hong, J.H. Boo, E.S. Jung, Y. Kim, J.Y. Baek, K.S. Kim, J.W. Cho, I. Mook-Jung, O-linked beta-N-acetylglucosaminidase inhibitor attenuates beta-amyloid plaque and rescues memory impairment, Neurobiol Aging, 34 (2013) 275-285.
[29] B. De Strooper, Nicastrin: gatekeeper of the gamma-secretase complex, Cell, 122 (2005) 318-320.
[30] S.A. Yuzwa, X. Shan, M.S. Macauley, T. Clark, Y. Skorobogatko, K. Vosseller, D.J. Vocadlo, Increasing O-GlcNAc slows neurodegeneration and stabilizes tau against aggregation, Nat Chem Biol, 8 (2012) 393-399.
[31] S.A. Yuzwa, X. Shan, B.A. Jones, G. Zhao, M.L. Woodward, X. Li, Y. Zhu, E.J. McEachern, M.A. Silverman, N.V. Watson, C.X. Gong, D.J. Vocadlo, Pharmacological inhibition of O-GlcNAcase (OGA) prevents cognitive decline and amyloid plaque formation in bigenic tau/APP mutant mice, Mol Neurodegener, 9 (2014) 42.
[32] M.E. Graham, M. Thaysen-Andersen, N. Bache, G.E. Craft, M.R. Larsen, N.H. Packer, P.J. Robinson, A novel post-translational modification in nerve terminals: O-linked N-acetylglucosamine phosphorylation, J Proteome Res, 10 (2011) 2725-2733.
[33] Y. Zhu, X. Shan, F. Safarpour, N. Erro Go, N. Li, A. Shan, M.C. Huang, M. Deen, V. Holicek, R. Ashmus, Z. Madden, S. Gorski, M.A. Silverman, D.J. Vocadlo, Pharmacological Inhibition of O-GlcNAcase Enhances Autophagy in Brain through an mTOR-Independent Pathway, ACS Chem Neurosci, (2018).
[34] E. Barone, F. Di Domenico, T. Cassano, A. Arena, A. Tramutola, M.A. Lavecchia, R. Coccia, D.A. Butterfield, M. Perluigi, Impairment of biliverdin reductase-A promotes brain insulin resistance in Alzheimer disease: A new paradigm, Free Radic Biol Med, 91 (2016) 127-142.

[35] F. Di Domenico, J.B. Owen, R. Sultana, R.A. Sowell, M. Perluigi, C. Cini, J. Cai, W.M. Pierce, D.A. Butterfield, The wheat germ agglutinin-fractionated proteome of subjects with Alzheimer's disease and mild cognitive impairment hippocampus and inferior parietal lobule: Implications for disease pathogenesis and progression, J Neurosci Res, 88 (2010) 3566-3577.
[36] J.B. Owen, F. Di Domenico, R. Sultana, M. Perluigi, C. Cini, W.M. Pierce, D.A. Butterfield, Proteomics-determined differences in the concanavalin-A-fractionated proteome of hippocampus and inferior parietal lobule in subjects with Alzheimer's disease and mild cognitive impairment: implications for progression of AD, J Proteome Res, 8 (2009) 471-482.
[37] S. Oddo, A. Caccamo, J.D. Shepherd, M.P. Murphy, T.E. Golde, R. Kayed, R. Metherate, M.P. Mattson, Y. Akbari, F.M. LaFerla, Triple-transgenic model of Alzheimer's disease with plaques and tangles: intracellular Abeta and synaptic dysfunction, Neuron, 39 (2003) 409-421.
[38] T. Cassano, A. Romano, T. Macheda, R. Colangeli, C.S. Cimmino, A. Petrella, F.M. LaFerla, V. Cuomo, S. Gaetani, Olfactory memory is impaired in a triple transgenic model of Alzheimer disease, Behav Brain Res, 224 (2011) 408-412.
[39] A. Romano, L. Pace, B. Tempesta, A.M. Lavecchia, T. Macheda, G. Bedse, A. Petrella, C. Cifani, G. Serviddio, G. Vendemiale, S. Gaetani, T. Cassano, Depressive-like behavior is paired to monoaminergic alteration in a murine model of Alzheimer's disease, Int J Neuropsychopharmacol, 18 (2014).
[40] N.E. Zachara, K. Vosseller, G.W. Hart, Detection and analysis of proteins modified by O-linked N-acetylglucosamine, Curr Protoc Mol Biol, Chapter 17 (2011) Unit 17 16.
[41] F. Ding, J. Yao, J.R. Rettberg, S. Chen, R.D. Brinton, Early decline in glucose transport and metabolism precedes shift to ketogenic system in female aging and Alzheimer's mouse brain: implication for bioenergetic intervention, PLoS One, 8 (2013) e79977.
[42] R.M. Nicholson, Y. Kusne, L.A. Nowak, F.M. LaFerla, E.M. Reiman, J. Valla, Regional cerebral glucose uptake in the 3xTG model of Alzheimer's disease highlights common regional vulnerability across AD mouse models, Brain Res, 1347 (2010) 179-185.
[43] K. Kaasik, S. Kivimae, J.J. Allen, R.J. Chalkley, Y. Huang, K. Baer, H. Kissel, A.L. Burlingame, K.M. Shokat, L.J. Ptacek, Y.H. Fu, Glucose sensor O-GlcNAcylation coordinates with phosphorylation to regulate circadian clock, Cell Metab, 17 (2013) 291-302.
[44] J.W. Bullen, J.L. Balsbaugh, D. Chanda, J. Shabanowitz, D.F. Hunt, D. Neumann, G.W. Hart, Cross-talk between two essential nutrient-sensitive enzymes: O-GlcNAc transferase (OGT) and AMP-activated protein kinase (AMPK), J Biol Chem, 289 (2014) 10592-10606.
[45] H.G. Seo, H.B. Kim, M.J. Kang, J.H. Ryum, E.C. Yi, J.W. Cho, Identification of the nuclear localisation signal of O-GlcNAc transferase and its nuclear import regulation, Sci Rep, 6 (2016) 34614.
[46] G.W. Hart, C. Slawson, G. Ramirez-Correa, O. Lagerlof, Cross talk between O-GlcNAcylation and phosphorylation: roles in signaling, transcription, and chronic disease, Annu Rev Biochem, 80 (2011) 825-858.
[47] K. Vosseller, L. Wells, M.D. Lane, G.W. Hart, Elevated nucleocytoplasmic glycosylation by O-GlcNAc results in insulin resistance associated with defects in Akt activation in 3T3-L1 adipocytes, Proc Natl Acad Sci U S A, 99 (2002) 5313-5318.
[48] F.I. Comer, G.W. Hart, O-Glycosylation of nuclear and cytosolic proteins. Dynamic interplay between O-GlcNAc and O-phosphate, J Biol Chem, 275 (2000) 29179-29182.
[49] Y.R. Yang, P.G. Suh, O-GlcNAcylation in cellular functions and human diseases, Adv Biol Regul, 54 (2014) 68-73.
[50] L.K. Kreppel, G.W. Hart, Regulation of a cytosolic and nuclear O-GlcNAc transferase. Role of the tetratricopeptide repeats, J Biol Chem, 274 (1999) 32015-32022.
[51] Z. Jahangir, W. Ahmad, K. Shabbiri, Alternate Phosphorylation/O-GlcNAc Modification on Human Insulin IRSs: A Road towards Impaired Insulin Signaling in Alzheimer and Diabetes, Adv Bioinformatics, 2014 (2014) 324753.

[52] D.A. Butterfield, S.S. Hardas, M.L. Lange, Oxidatively modified glyceraldehyde-3-phosphate dehydrogenase (GAPDH) and Alzheimer's disease: many pathways to neurodegeneration, J Alzheimers Dis, 20 (2010) 369-393.
[53] J. Seo, J. Jeong, Y.M. Kim, N. Hwang, E. Paek, K.J. Lee, Strategy for comprehensive identification of post-translational modifications in cellular proteins, including low abundant modifications: application to glyceraldehyde-3-phosphate dehydrogenase, J Proteome Res, 7 (2008) 587-602.
[54] N. Reiss, J. Hermon, A. Oplatka, Z. Naor, Interaction of purified protein kinase C with key proteins of energy metabolism and cellular motility, Biochem Mol Biol Int, 38 (1996) 711-719.
[55] N. Reiss, H. Kanety, J. Schlessinger, Five enzymes of the glycolytic pathway serve as substrates for purified epidermal-growth-factor-receptor kinase, Biochem J, 239 (1986) 691-697.
[56] Y. Bian, C. Song, K. Cheng, M. Dong, F. Wang, J. Huang, D. Sun, L. Wang, M. Ye, H. Zou, An enzyme assisted RP-RPLC approach for in-depth analysis of human liver phosphoproteome, J Proteomics, 96 (2014) 253-262.
[57] H. Zhou, S. Di Palma, C. Preisinger, M. Peng, A.N. Polat, A.J. Heck, S. Mohammed, Toward a comprehensive characterization of a human cancer cell phosphoproteome, J Proteome Res, 12 (2013) 260-271.
[58] Y.V. Skorobogatko, J. Deuso, J. Adolf-Bryfogle, M.G. Nowak, Y. Gong, C.F. Lippa, K. Vosseller, Human Alzheimer's disease synaptic O-GlcNAc site mapping and iTRAQ expression proteomics with ion trap mass spectrometry, Amino Acids, 40 (2011) 765-779.
[59] F. Di Domenico, R. Sultana, E. Barone, M. Perluigi, C. Cini, C. Mancuso, J. Cai, W.M. Pierce, D.A. Butterfield, Quantitative proteomics analysis of phosphorylated proteins in the hippocampus of Alzheimer's disease subjects, J Proteomics, 74 (2011) 1091-1103.
[60] M. Perluigi, E. Barone, F. Di Domenico, D.A. Butterfield, Aberrant protein phosphorylation in Alzheimer disease brain disturbs pro-survival and cell death pathways, Biochim Biophys Acta, 1862 (2016) 1871-1882.
[61] S. Zahid, M. Oellerich, A.R. Asif, N. Ahmed, Phosphoproteome profiling of substantia nigra and cortex regions of Alzheimer's disease patients, J Neurochem, 121 (2012) 954-963.
[62] D.A. Butterfield, L. Gu, F. Di Domenico, R.A. Robinson, Mass spectrometry and redox proteomics: applications in disease, Mass Spectrom Rev, 33 (2014) 277-301.
[63] M.Y. Cha, H.J. Cho, C. Kim, Y.O. Jung, M.J. Kang, M.E. Murray, H.S. Hong, Y.J. Choi, H. Choi, D.K. Kim, H. Choi, J. Kim, D.W. Dickson, H.K. Song, J.W. Cho, E.C. Yi, J. Kim, S.M. Jin, I. Mook-Jung, Mitochondrial ATP synthase activity is impaired by suppressed O-GlcNAcylation in Alzheimer's disease, Hum Mol Genet, 24 (2015) 6492-6504.
[64] G. Bedse, F. Di Domenico, G. Serviddio, T. Cassano, Aberrant insulin signaling in Alzheimer's disease: current knowledge, Front Neurosci, 9 (2015) 204.
[65] R. Pardeshi, N. Bolshette, K. Gadhave, A. Ahire, S. Ahmed, T. Cassano, V.B. Gupta, M. Lahkar, Insulin signaling: An opportunistic target to minify the risk of Alzheimer's disease, Psychoneuroendocrinology, 83 (2017) 159-171.
[66] S.A. Whelan, W.B. Dias, L. Thiruneelakantapillai, M.D. Lane, G.W. Hart, Regulation of insulin receptor substrate 1 (IRS-1)/AKT kinase-mediated insulin signaling by O-Linked beta-N-acetylglucosamine in 3T3-L1 adipocytes, J Biol Chem, 285 (2010) 5204-5211.
[67] J.C. Bruning, D. Gautam, D.J. Burks, J. Gillette, M. Schubert, P.C. Orban, R. Klein, W. Krone, D. Muller-Wieland, C.R. Kahn, Role of brain insulin receptor in control of body weight and reproduction, Science, 289 (2000) 2122-2125.
[68] T. Issad, E. Masson, P. Pagesy, O-GlcNAc modification, insulin signaling and diabetic complications, Diabetes Metab, 36 (2010) 423-435.
[69] C. Phoomak, K. Vaeteewoottacharn, A. Silsirivanit, C. Saengboonmee, W. Seubwai, K. Sawanyawisuth, C. Wongkham, S. Wongkham, High glucose levels boost the aggressiveness of highly metastatic cholangiocarcinoma cells via O-GlcNAcylation, Sci Rep, 7 (2017) 43842.

[70] L.E. Ball, M.N. Berkaw, M.G. Buse, Identification of the major site of O-linked beta-N-acetylglucosamine modification in the C terminus of insulin receptor substrate-1, Mol Cell Proteomics, 5 (2006) 313-323.
[71] J. Shi, J.H. Gu, C.L. Dai, J. Gu, X. Jin, J. Sun, K. Iqbal, F. Liu, C.X. Gong, O-GlcNAcylation regulates ischemia-induced neuronal apoptosis through AKT signaling, Sci Rep, 5 (2015) 14500.
[72] J. Shi, S. Wu, C.L. Dai, Y. Li, I. Grundke-Iqbal, K. Iqbal, F. Liu, C.X. Gong, Diverse regulation of AKT and GSK-3beta by O-GlcNAcylation in various types of cells, FEBS Lett, 586 (2012) 2443-2450.
[73] F. Zhang, B. Su, C. Wang, S.L. Siedlak, S. Mondragon-Rodriguez, H.G. Lee, X. Wang, G. Perry, X. Zhu, Posttranslational modifications of alpha-tubulin in alzheimer disease, Transl Neurodegener, 4 (2015) 9.
[74] Y. Song, S.T. Brady, Post-translational modifications of tubulin: pathways to functional diversity of microtubules, Trends Cell Biol, 25 (2015) 125-136.
[75] D. Wloga, J. Gaertig, Post-translational modifications of microtubules, J Cell Sci, 123 (2010) 3447-3455.
[76] R.N. Cole, G.W. Hart, Cytosolic O-glycosylation is abundant in nerve terminals, J Neurochem, 79 (2001) 1080-1089.
[77] J.C. Triplett, A.M. Swomley, J. Cai, J.B. Klein, D.A. Butterfield, Quantitative phosphoproteomic analyses of the inferior parietal lobule from three different pathological stages of Alzheimer's disease, J Alzheimers Dis, 49 (2016) 45-62.
[78] S. Petratos, Q.X. Li, A.J. George, X. Hou, M.L. Kerr, S.E. Unabia, I. Hatzinisiriou, D. Maksel, M.I. Aguilar, D.H. Small, The beta-amyloid protein of Alzheimer's disease increases neuronal CRMP-2 phosphorylation by a Rho-GTP mechanism, Brain, 131 (2008) 90-108.
[79] T. Yoshimura, Y. Kawano, N. Arimura, S. Kawabata, A. Kikuchi, K. Kaibuchi, GSK-3beta regulates phosphorylation of CRMP-2 and neuronal polarity, Cell, 120 (2005) 137-149.
[80] A. Tramutola, C. Lanzillotta, F. Di Domenico, Targeting mTOR to reduce Alzheimer-related cognitive decline: from current hits to future therapies, Expert Rev Neurother, 17 (2017) 33-45.
[81] F. Di Domenico, E. Barone, M. Perluigi, D.A. Butterfield, The Triangle of Death in Alzheimer's Disease Brain: The Aberrant Cross-Talk Among Energy Metabolism, Mammalian Target of Rapamycin Signaling, and Protein Homeostasis Revealed by Redox Proteomics, Antioxid Redox Signal, 26 (2017) 364-387.
[82] D.J. Colacurcio, A. Pensalfini, Y. Jiang, R.A. Nixon, Dysfunction of autophagy and endosomal-lysosomal pathways: Roles in pathogenesis of Down syndrome and Alzheimer's Disease, Free Radic Biol Med, 114 (2018) 40-51.
[83] M. Perluigi, F. Di Domenico, D.A. Butterfield, mTOR signaling in aging and neurodegeneration: At the crossroad between metabolism dysfunction and impairment of autophagy, Neurobiol Dis, 84 (2015) 39-49.
[84] W.Y. Wani, M. Boyer-Guittaut, M. Dodson, J. Chatham, V. Darley-Usmar, J. Zhang, Regulation of autophagy by protein post-translational modification, Lab Invest, 95 (2015) 14-25.
[85] A. Tramutola, J.C. Triplett, F. Di Domenico, D.M. Niedowicz, M.P. Murphy, R. Coccia, M. Perluigi, D.A. Butterfield, Alteration of mTOR signaling occurs early in the progression of Alzheimer disease (AD): analysis of brain from subjects with pre-clinical AD, amnestic mild cognitive impairment and late-stage AD, J Neurochem, 133 (2015) 739-749.
[86] D. Szklarczyk, J.H. Morris, H. Cook, M. Kuhn, S. Wyder, M. Simonovic, A. Santos, N.T. Doncheva, A. Roth, P. Bork, L.J. Jensen, C. von Mering, The STRING database in 2017: quality-controlled protein-protein association networks, made broadly accessible, Nucleic Acids Res, 45 (2017) D362-D368.
[87] L.J. Jensen, M. Kuhn, M. Stark, S. Chaffron, C. Creevey, J. Muller, T. Doerks, P. Julien, A. Roth, M. Simonovic, P. Bork, C. von Mering, STRING 8-a global view on proteins and their functional interactions in 630 organisms, Nucleic Acids Research, 37 (2009) D412-D416.

Figure legends

Figure 1. Protein levels and localization of *O*-GlcNAcylated and phosphorylated (Ser/Thr) proteins in hippocampus of 3×Tg-AD and Non-Tg mice. Representative western Blot (A) showing on the left the protein *O*-GlcNAcylation profile detected by RL2 and CTD110.6 antibodies used independently and on the right the total levels of protein *O*-GlcNAcylation of the hippocampus from of 3×Tg-AD mice at 12 months compared with their age matched Non-Tg mice. Quantification of the Western Blot (B) indicate a significant reduction in *O*-GlcNAcylation in 3×Tg-AD mice at 12 months compared with Non-Tg. Representative immunofluorescence images (D) showing O-GlcNAc signal (1-4) and p-Ser/Thr (5-8) in the CA3 region of the hippocampus (D.1) of 3×Tg-AD and Non-Tg at 12 months. DAPI (blue in panel C, 1-8) was used to identify cell nuclei. Quantification of immunofluorescence staining (C) for p-Ser/Thr indicate a significant increase of total phosphorylation in the CA3 region of the hippocampus of 3×Tg-AD mice at 12 months compared with Non-Tg. Correlation analysis (E) between total protein *O*-GlcNAcylation and protein phosphorylation of 3xTg-AD (black) and Non-Tg (white) animals (3xTg-AD - R squared= 0.852, p= 0.025). Densitometric values shown in the bar graph are the mean ± SEM of 6 individual mouse samples per each group normalized on total load and are given as a percentage of Non-Tg, set as 100%. Statistical significance was determined using Unpaired t test (* $p<0.05$)

Figure 2. Protein levels and activation status of the enzymes involved in the *O*-GlcNAcylation process in the hippocampus of 3×Tg-AD and Non-Tg mice. Panel A and B: representative western blot (A) and quantification of total protein levels (B) and activity assay (B) of OGA in 3×Tg-AD mice at 12 months compared with Non-Tg. Panel C and D: representative western blot (C) obtained by immunoprecipitation assay for OGT (C). Quantification of *O*-GlcNAcylation, total phosphorylation on Ser/Thr residues and total protein levels (D) of OGT in 3×Tg-AD mice at 12 months compared with Non-Tg. Densitometric values shown in the bar graph are the mean ± SEM of 6 individual mouse samples per each group normalized on total load (A-B) and total OGT protein levels (C-D) and are given as a percentage of Non-Tg, set as 100%. Statistical significance was determined using Unpaired t test (* $p<0.05$)

Figure 3. Proteomic profile of representative 2D-Blot with all identified proteins (A) that are differentially *O*-glycosylated in 3×Tg-AD mice compared with Non-Tg. In panel B and C a representative 2D-Blot of the glyco-proteomic profile in the hippocampus of Non-Tg and 3×Tg-AD mice.

Figure 4. Immunoprecipitation and quantification of Ulk1 (A-B) and Drp-2 (C-D) modified by *O*-GlcNAc and p-(Ser/Thr). Protein total p-(ser/Thr) and *O*-GlcNAc of Ulk1 (A, B), Drp-2 (C, D), Gapdh (E, F) and Eno1 (G, H) were detected by immunoprecipitation of 3×Tg-AD mouse compared with Non-Tg. Densitometric values shown in the bar graph are the mean ± SEM of 6 individual mouse samples per each group normalized on Ulk1, Drp-2, Eno1 and Gapdh total protein levels from IP experiments and are given as a percentage of Non-Tg, set as 100%. Statistical significance was determined using Unpaired t test (* $p<0.05$, ** $p<0.01$)

Figure 5. *O*-GlcNAcylation of insulin signaling components. Panel A, B and C: Representative western blot (A) showing phosphorylation of IRS1 on Ser 636 residue. Protein bound O-GlcNAc of IRS1 (B) are detected by immunoprecipitation in 3×Tg-AD compared with Non-Tg mice. Quantification of the Western Blot and the Immunoprecipitation (C) of IRS1 in the hippocampus of 3×Tg-AD and Non-Tg. Panel D, E and F: Representative western blot (D) showing phosphorylation of Akt on Ser 473 residue. Protein bound *O*-GlcNAc of Akt (E) are detected by immunoprecipitation in 3×Tg-AD compared with Non-Tg mice. Quantification of the Western Blot and the Immunoprecipitation (F) of Akt in the hippocampus of 3×Tg-AD and Non-Tg. Densitometric values shown in the bar graph are the mean ± SEM of 6 individual mouse samples per each group normalized respectively on IRS1 and Akt protein levels from IP and are given as a percentage of Non-Tg, set as 100%. Statistical significance was determined using Unpaired t test (*$p<0.05$, *** $p<0.001$)

Figure 6. Protein-protein interaction network and enrichment analysis. Combined screenshot from the STRING website, showing results obtained upon entering a set of 14 proteins that result differentially *O*-GlcNAcylated in 3×Tg-AD. In the top inset, two enriched function are described. The bottom inset is showing a reported enrichment of functional connections among the set of proteins, and statistical enrichments detected in functional subsystems. Different coloured edges represent the existence of different type of evidence. A green line indicates neighbourhood evidence; a blue line, gene co-occurrence; a yellow line, text mining; a purple line, experimental evidence. The software calculates an index of interaction confidence from 0 to 1 based on predicted protein interactions analysis and experimentally published protein interaction data. In details, the table show stronger interactions for enzymes of glycolysis and Krebs cycle. A potential interaction is reported between 14-3-3 epsilon protein and Ran protein. The interaction between Gapdh and α-tubulin is also reported. Lastly, a predicted interaction is reported for Eno1 and Drp-2 proteins.

Table 1. List of identified O-GlcNAc proteins in Hippocampus of 3×Tg-AD and Non-Tg mice.

Spot N.	Protein	Uniprot N.	Fold decrease 3xTg-AD vs Non-Tg	p-value	O-GlcNac*	Score	Cvg	Pep.
0303	Elongin-C (Eloc)	P83940	4.1	0.031	/	2.01	17.86	1
0503	Glyceraldehyde-3-phosphate dehydrogenase (Gapdh)	P16858	7.1	0.045	/	4.24	14.71	3
2103	GTP-binding nuclear protein Ran (Ran)	P62827	5.2	0.017	/	1.98	13.43	3
4108	Serine/threonine-protein kinase Ulk1 (ULK1)	O70405	2.1	0.033	Thr327; Ser330	1.87	1.52	1
4502	Putative ATP-dependent RNA helicase TDRD9 (TDRD9)	Q14BI7	4.1	0.041	Ser1201; Ser1203	5.7	1.37	1
4503	Myosin phosphatase Rho-interacting protein (Mprip)	P97434	5.0	0.013	Ser485; Ser491	2.71	1.76	1
4804	Tubulin alpha-1C chain (Tuba1c)	P68373	10.0	0.048	/	2.73	3.34	1
5407	Alpha-enolase (Eno1)	P17182	9.0	0.044	/	73.2	41.9	16
5702	Dihydropyrimidinase-related protein 2 (Drp-2)	O08553	2.0	0.037	/	2.4	7.87	4
6203	Malate dehydrogenase, (Mdh)	P08249	4.3	0.05	/	26.1	24.5	8
6802	Contactin-associated protein-like 2 (Cntnap2)	Q9CPW0	14.2	0.028	Ser543; Thr994	2.59	2.85	2
6905	Coiled-coil domain-containing protein 63 (Ccdc63)	Q8CDV6	2.1	0.022	Thr423; Ser432	2.42	3.05	1
8114	14-3-3 protein epsilon (14-3-3E)	P62259	6.25	0.044	/	23.39	27.45	7
9701	Neurofilament light polypeptide (NF-L)	P08551	3.3	0.05	/	3.98	11.23	7

* Ser/Thr residues with O-linked GlcNAc

Highlights

- Reduced glucose uptake in AD lead to the alteration of the hexosamine biosynthetic pathway and to flawed protein *O*-GlcNAcylation
- O-GlcNacylation is mutually related with phosphorylation having the ability to modulate various signaling pathways involved in neuron development and homeostasis
- In AD brain protein O-GlcNAcylation levels, including that of tau and APP, appear to dramatically decrease as phosphorylation increase
- Our data demonstrated the reduction for total and protein specific O-GlcNAcylation in 3xTg-AD mice compared with Non-Tg
- We identified the reduced O-GlcNAcylation of key proteins involved in brain function and homeostasis whose alteration may contribute to AD development and progression.

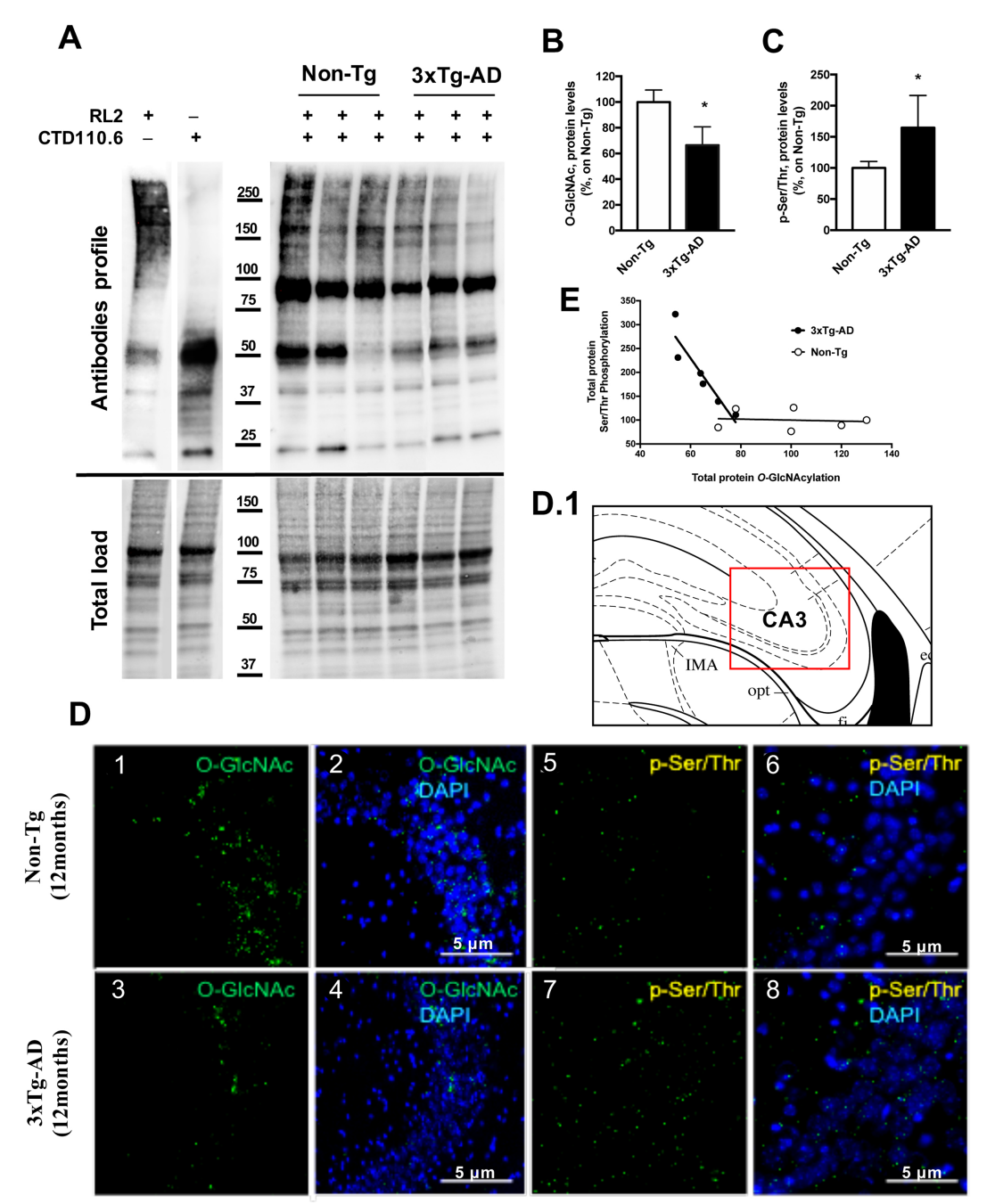
A
Non-Tg
3xTg-AD
RL2
CTD110.6
Antibodies profile
Total load
250
150
100
75
50
37
25
B
O-GlcNAc, protein levels (%, on Non-Tg)
Non-Tg
3xTg-AD
C
p-Ser/Thr, protein levels (%, on Non-Tg)
E
Total protein Ser/Thr Phosphorylation
3xTg-AD
Non-Tg
Total protein O-GlcNAcylation
D.1
CA3
IMA
opt
D
Non-Tg (12months)
3xTg-AD (12months)
1 O-GlcNAc
2 O-GlcNAc DAPI
3 O-GlcNAc
4 O-GlcNAc DAPI
5 p-Ser/Thr
6 p-Ser/Thr DAPI
7 p-Ser/Thr
8 p-Ser/Thr DAPI
5 µm

Figure 1

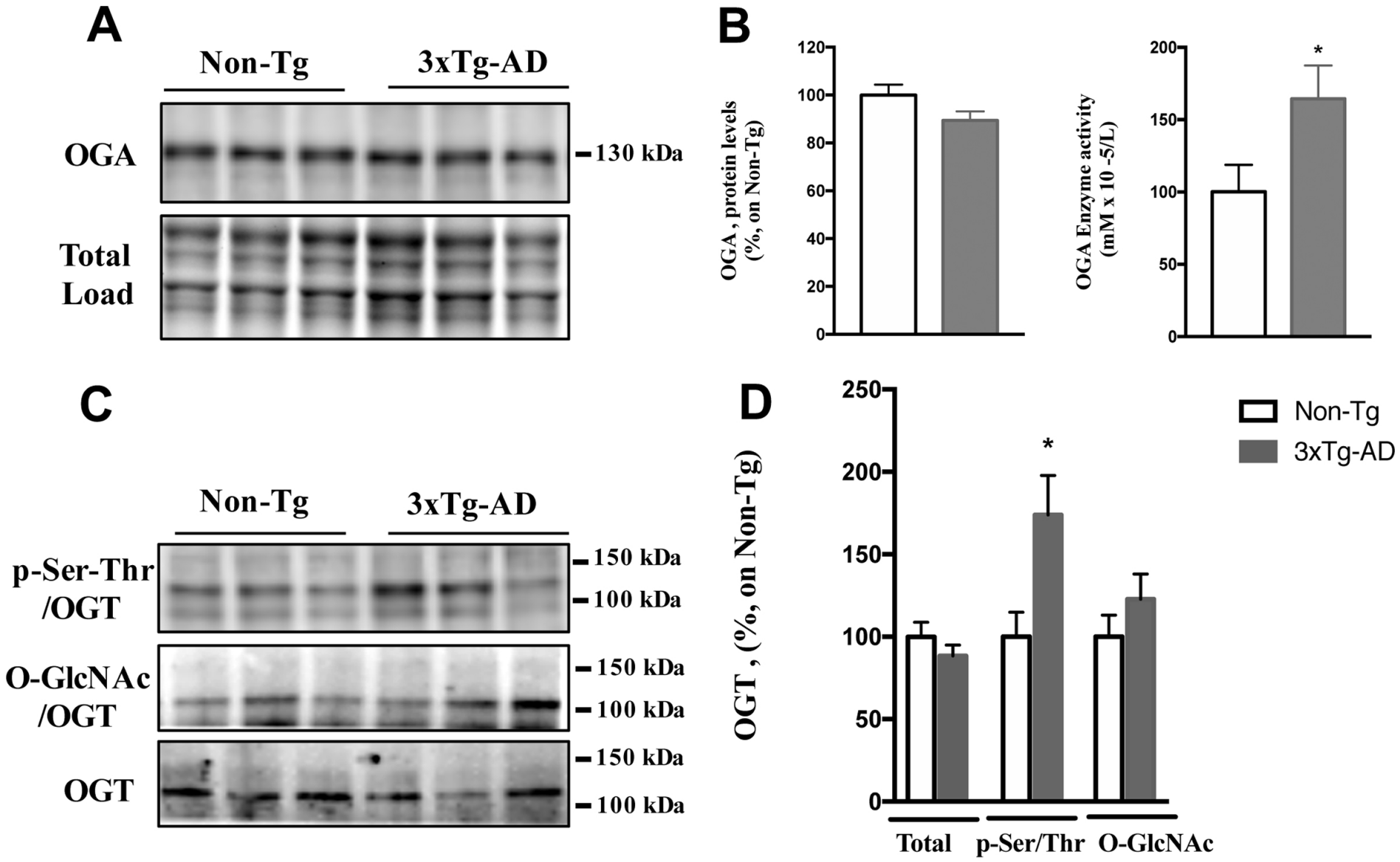
A
Non-Tg
3xTg-AD
OGA
130 kDa
Total Load
B
OGA, protein levels (%, on Non-Tg)
120
100
80
60
40
20
0
OGA Enzyme activity (mM x 10 -5/L)
200
150
100
50
0
*
C
Non-Tg
3xTg-AD
p-Ser-Thr /OGT
150 kDa
100 kDa
O-GlcNAc /OGT
150 kDa
100 kDa
OGT
150 kDa
100 kDa
D
OGT, (%, on Non-Tg)
250
200
150
100
50
0
*
Non-Tg
3xTg-AD
Total
p-Ser/Thr
O-GlcNAc

Figure 2

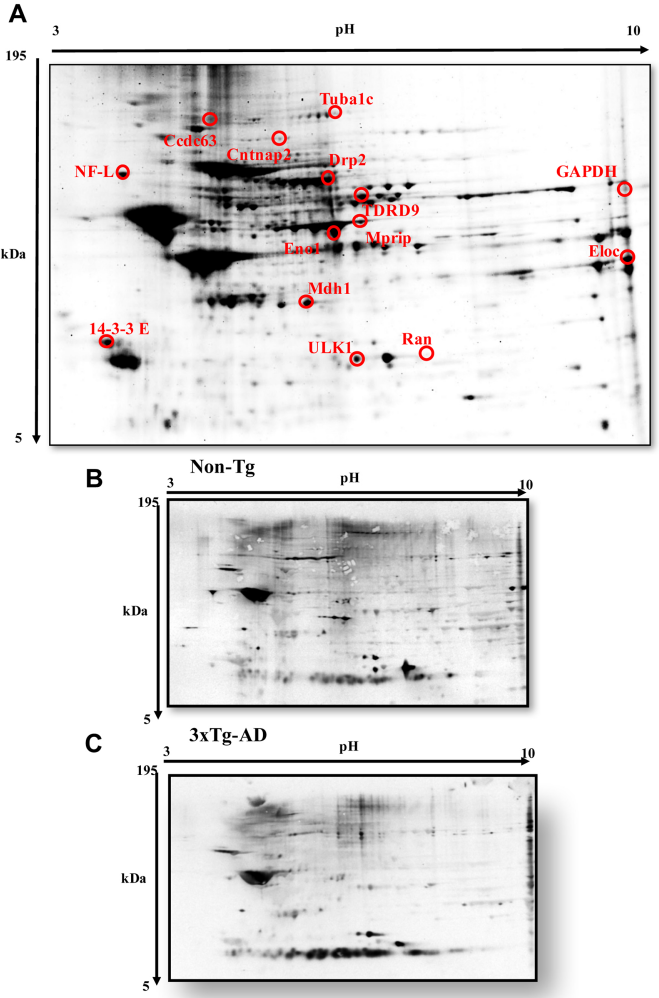
A
3
pH
10
195
kDa
5
Tuba1c
Ccdc63
Cntnap2
Drp2
NF-L
GAPDH
TDRD9
Mprip
Eno1
Eloc
Mdh1
14-3-3 E
ULK1
Ran
B
Non-Tg
3
pH
10
195
kDa
5
C
3xTg-AD
3
pH
10
195
kDa
5

Figure 3

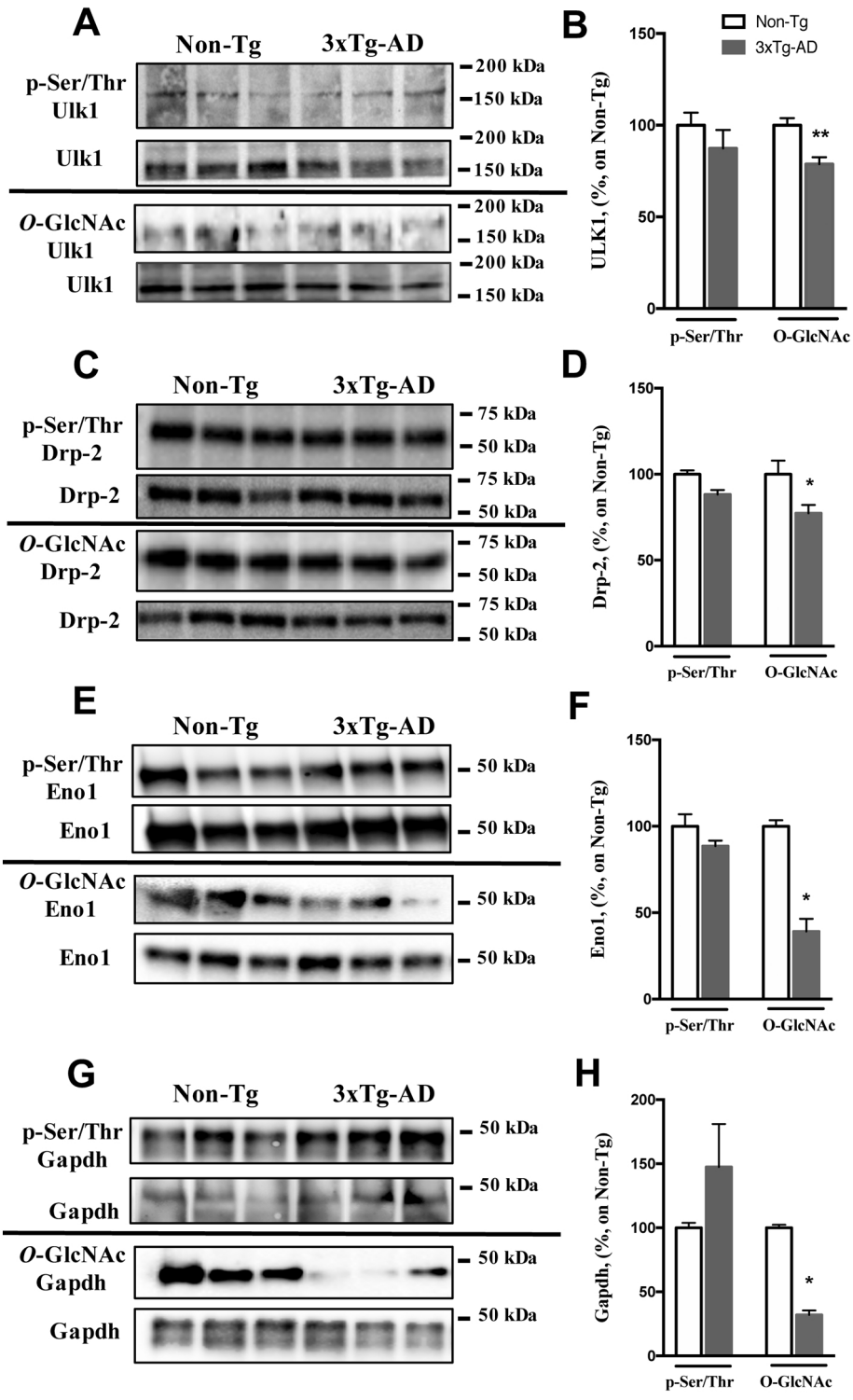
A
Non-Tg
3xTg-AD
p-Ser/Thr Ulk1
Ulk1
O-GlcNAc Ulk1
Ulk1
200 kDa
150 kDa
B
Non-Tg
3xTg-AD
ULK1, (%, on Non-Tg)
150
100
50
0
**
p-Ser/Thr
O-GlcNAc
C
Non-Tg
3xTg-AD
p-Ser/Thr Drp-2
Drp-2
O-GlcNAc Drp-2
Drp-2
75 kDa
50 kDa
D
Drp-2, (%, on Non-Tg)
150
100
50
0
*
p-Ser/Thr
O-GlcNAc
E
Non-Tg
3xTg-AD
p-Ser/Thr Eno1
Eno1
O-GlcNAc Eno1
Eno1
50 kDa
F
Eno1, (%, on Non-Tg)
150
100
50
0
*
p-Ser/Thr
O-GlcNAc
G
Non-Tg
3xTg-AD
p-Ser/Thr Gapdh
Gapdh
O-GlcNAc Gapdh
Gapdh
50 kDa
H
Gapdh, (%, on Non-Tg)
200
150
100
50
0
*
p-Ser/Thr
O-GlcNAc

Figure 4

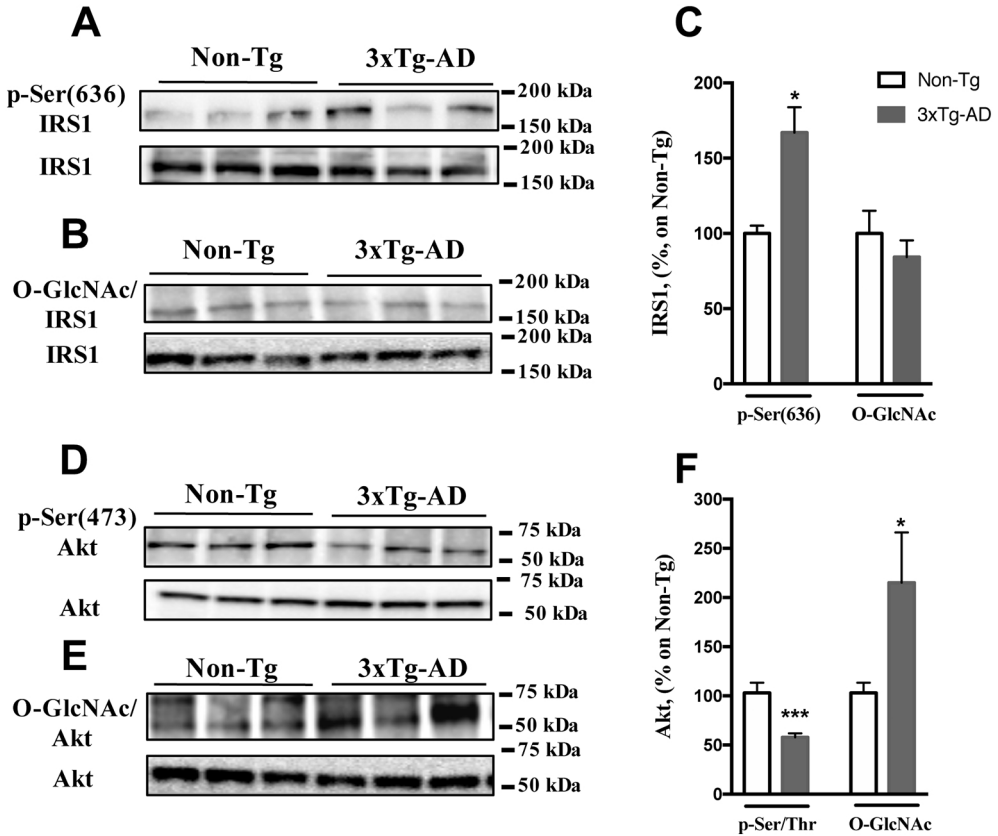
A
Non-Tg
3xTg-AD
p-Ser(636) IRS1
IRS1
200 kDa
150 kDa
200 kDa
150 kDa
B
Non-Tg
3xTg-AD
O-GlcNAc/ IRS1
IRS1
200 kDa
150 kDa
200 kDa
150 kDa
C
Non-Tg
3xTg-AD
IRS1, (%, on Non-Tg)
200
150
100
50
0
*
p-Ser(636)
O-GlcNAc
D
Non-Tg
3xTg-AD
p-Ser(473) Akt
Akt
75 kDa
50 kDa
75 kDa
50 kDa
E
Non-Tg
3xTg-AD
O-GlcNAc/ Akt
Akt
75 kDa
50 kDa
75 kDa
50 kDa
F
Akt, (% on Non-Tg)
300
250
200
150
100
50
0
***
*
p-Ser/Thr
O-GlcNAc

Figure 5

Network Stats

number of nodes:	14	expected number of edges:	3
number of edges:	5	PPI enrichment p-value:	0.138
average node degree:	0.714	*your network does **not** have significantly more interactions than expected (what does that mean?)*	
avg. local clustering coefficient:	0.381		

Functional enrichments in your network

Biological Process (GO)

pathway ID	*pathway description*	*count in gene set*	*false discovery rate*
GO:0021761	limbic system development	5	2.91e-05
GO:0030900	forebrain development	6	0.000219
GO:0021766	hippocampus development	4	0.000329
GO:0021537	telencephalon development	5	0.000546
GO:0007420	brain development	6	0.00254
			(more ...)

Cellular Component (GO)

pathway ID	*pathway description*	*count in gene set*	*false discovery rate*
GO:0043209	myelin sheath	5	0.000117
GO:0005829	cytosol	8	0.000787
GO:0005856	cytoskeleton	8	0.000787
GO:0015630	microtubule cytoskeleton	6	0.00417
GO:0005737	cytoplasm	13	0.00975
			(more ...)

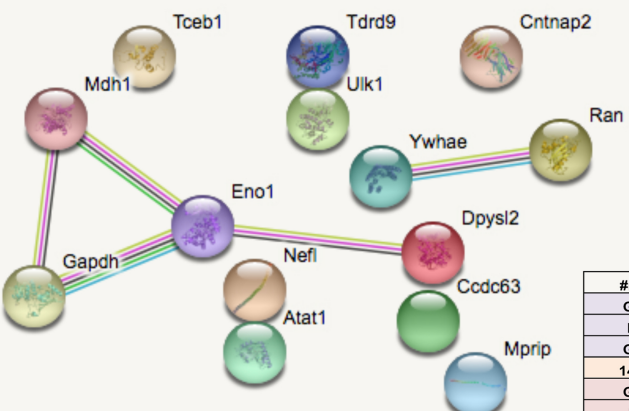

Proteins interactions table

#node1	node2	combined_score
Gapdh	Eno1	0.994
Mdh1	Eno1	0.768
Gapdh	Mdh1	0.709
14-3-3 E	Ran	0.603
Gapdh	Tuba1c	0.533
Eno1	Dpysl2	0.454

Figure 6